AD-A055 792 UNITED TECHNOLOGIES RESEARCH CENTER EAST HARTFORD CONN F/G 20/6
INVESTIGATION OF PLASMA PROCESSES IN ELECTRONIC TRANSITION LASE--ETC(U).
JUL 78 W L NIGHAN N00014-76-C-0847
UNCLASSIFIED UTRC/R78-922617-3 NL

1 OF 1
ADA
055792

END
DATE
FILMED
8-78
DDC

Unclassified

SECURITY CLASSIFICATION OF THIS PAGE (When Data Entered)

REPORT DOCUMENTATION PAGE

READ INSTRUCTIONS BEFORE COMPLETING FORM

1. REPORT NUMBER: R78-922617-3	2. GOVT ACCESSION NO. (9)
3. RECIPIENT'S CATALOG NUMBER	
4. TITLE (and Subtitle): (6) Investigation of Plasma Processes in Electronic Transition Lasers.	5. TYPE OF REPORT & PERIOD COVERED: Technical Report. 1 Jul 77-1 Jul 78
	6. PERFORMING ORG. REPORT NUMBER: R78-922617-3 (14) UTRC
7. AUTHOR(s): (10) William L. Nighan	8. CONTRACT OR GRANT NUMBER(s): (15) N00014-76-C-0847
9. PERFORMING ORGANIZATION NAME AND ADDRESS: United Technologies Research Center, Silver Lane, East Hartford, CT 06108	10. PROGRAM ELEMENT, PROJECT, TASK AREA & WORK UNIT NUMBERS: (11) 1 Jul 78
11. CONTROLLING OFFICE NAME AND ADDRESS: Office of Naval Research, Physics Program Office, 800 N. Quincy Street, Arlington, VA 22717	12. REPORT DATE: July 1, 1978
	13. NUMBER OF PAGES: 74 (12) 80p.
14. MONITORING AGENCY NAME & ADDRESS (if different from Controlling Office)	15. SECURITY CLASS. (of this report): Unclassified
	15a. DECLASSIFICATION/DOWNGRADING SCHEDULE

16. DISTRIBUTION STATEMENT (of this Report)

Approved for public release; distribution unlimited. Reproduction in whole or in part is permitted for any purpose of the United States Government.

17. DISTRIBUTION STATEMENT (of the abstract entered in Block 20, if different from Report)

18. SUPPLEMENTARY NOTES

To be published in the IEEE Journal of Quantum Electronics

19. KEY WORDS (Continue on reverse side if necessary and identify by block number)

Rare gas-halide lasers, KrF* lasers, electronic transition lasers, plasma processes in KrF* lasers, electron-beam controlled KrF* laser discharges, electron collision processes in KrF* lasers, instability in KrF* laser discharges, e-F_2 collisions in KrF* lasers

20. ABSTRACT (Continue on reverse side if necessary and identify by block number)

This paper presents the results of an analysis of plasma properties in an electron-beam controlled KrF* laser discharge. In this study special emphasis is placed on establishing the relationship among the numerous kinetic processes influencing the populations of excited species in the laser medium. Important reactions controlling the coupled populations of rare-gas metastable states and higher excited states are discussed in detail, along with the resultant effect of these reactions on KrF* formation efficiency. It is shown

DD FORM 1 JAN 73 1473 EDITION OF 1 NOV 65 IS OBSOLETE

S/N 0102-LF-014-6601

Unclassified

SECURITY CLASSIFICATION OF THIS PAGE (When Data Entered)

that the rare-gas monohalide production efficiency is approximately 20 percent under typical conditions, and that no single reaction dominates either production or loss of KrF*. In addition, the very important role of halogen molecule dissociation is treated and the resultant effects of dissociation on the temporal variations of plasma properties and on plasma stability are analyzed.

Reprints of related publications are included in the Appendix to this report.

Report R78-922617-3

INVESTIGATION OF PLASMA PROCESSES IN ELECTRONIC TRANSITION LASERS

William L. Nighan

Technical Report
July 1, 1978

Sponsored by the Office of Naval Research
under Contract N00014-76-C-0847

United Technologies Research Center
East Hartford, Connecticut 06108

PREFACE

Under the present ONR Contract, United Technologies Research Center is conducting an analytical investigation of plasma processes in electrically excited rare-gas halide lasers, with particular emphasis directed toward electron-beam controlled laser discharges. This work is being carried out in coordination with a Corporate sponsored experimental program. Emphasis in this investigation is being placed on identification of fundamental processes influencing electron energy transfer, charged particle production and loss, metastable production and loss, and plasma stability.

The present technical report is based upon a paper entitled, "Plasma Processes in Electron-Beam Controlled Rare-Gas Halide Lasers", which will be published in the IEEE Journal of Quantum Electronics. Reprints of recently published papers are also included in an appendix.

Investigation of Plasma Processes in Electronic Transition Lasers

TABLE OF CONTENTS

PLASMA PROCESSES IN ELECTRON-BEAM CONTROLLED RARE-GAS HALIDE LASERS*

by

William L. Nighan
United Technologies Research Center
East Hartford, CT 06108

ABSTRACT

This paper presents the results of an analysis of plasma properties in an electron-beam controlled KrF* laser discharge. In this study special emphasis is placed on establishing the relationship among the numerous kinetic processes influencing the populations of excited species in the laser medium. Important reactions controlling the coupled populations of rare-gas metastable states and higher excited states are discussed in detail, along with the resultant effect of these reactions on KrF* formation efficiency. It is shown that the rare-gas monohalide production efficiency is approximately 20 percent under typical conditions, and that no single reaction dominates either production or loss of KrF*. In addition, the very important role of halogen molecule dissociation is treated and the resultant effects of dissociation on the temporal variations of plasma properties and on plasma stability are analyzed.

*Portions of this work were supported by the Office of Naval Research.

I. INTRODUCTION

The electrically excited rare-gas halide laser is the first short-wavelength laser which appears capable of scaling to high pulse energy and high average power. Electrical-optical energy conversion efficiency of approximately 10 percent has been attained[1] for a single-pulse KrF* laser (λ = 248 nm), the most efficient of the rare-gas halide class. There are numerous applications for efficient uv and/or visible wavelength lasers, and for this reason these new laser systems have become the subject of increasing attention.[2] At the time the potential of rare-gas monohalides as laser molecules was first recognized[3] their properties were essentially unknown. For this reason early emphasis was placed on development of a thorough understanding of the structure of such molecules and their reaction kinetics. These efforts have resulted in a relatively complete understanding of rare-gas halide emission spectra[4], and of the dominant formation and quenching processes of these molecules.[5] Additionally, detailed modeling of kinetic processes has provided the insight required to identify optimum conditions for rare-gas halide laser operation.[1,6,7]

The plasma medium typical of these lasers is created in a near atmospheric pressure rare-gas mixture containing a small (< 1 percent) fractional concentration of a halogen-bearing molecule. Pulsed electrical excitation is provided either by a beam of high energy electrons or by an electric discharge in a manner generally similar to that typical of CO_2 lasers.[8,9] However, there are several significant features which differentiate rare-gas halide lasers from their ir molecular laser counterparts. These include: (1) a high concentration

of "alkali-like" rare gas metastable atoms which, because of their chemical activity,[3] exert a dominant influence on all aspects of plasma behavior; (2) a major constituent (the molecular halogen) which dissociates rapidly under the conditions required for laser operation, an effect resulting in very important temporal changes in the gas mixture; and (3) an electron density which is above the level at which electron-electron collisions become important, with the result that the plasma cannot be considered weakly ionized. This paper presents the results of a theoretical investigation of these and related plasma processes for conditions representative of KrF* lasers. Special emphasis is placed on establishing the relationship among the numerous kinetic processes which influence the populations of various excited species. The results presented are qualitatively similar for all rare-gas halide lasers, and should provide useful information relevant to other promising excimer lasers as well.

Section II summarizes the basic processes contributing to the production and loss of rare-gas metastable atoms and of KrF* molecules. Particular emphasis is placed on analysis of electron-atom excitation and ionization, especially the dependence of rate coefficients for these processes on the fractional concentration of electronically excited species and of electrons. In addition, the potential importance of vibrational excitation and dissociation of F_2 by low energy electron impact and of electron attachment to vibrationally excited F_2 are discussed. The results of an analysis of plasma properties in an electron-beam controlled KrF* laser discharge are presented in Section III. Therein the important reactions controlling the coupled populations of rare-gas metastable states and higher excited states are discussed in detail along with the resultant effect

of these reactions on KrF* formation efficiency. In addition, the very important role of halogen molecule dissociation is treated and the resultant effect of dissociation on plasma stability is analyzed. Important processes requiring improved understanding prior to successful application of rare-gas halide lasers are discussed in Section IV.

II. PLASMA PROCESSES

A. KrF* Formation and Loss

Rare-gas halide lasers have been excited successfully both by electron beams and by electric discharges[1]. In the latter case either fast pulse discharges or electron-beam controlled discharges have been used. Rare-gas monohalide molecule formation proceeds by way of generally similar processes in each case. The more important features of the KrF* formation and loss sequence in a nominally atmospheric pressure Ar-Kr-F_2 gas mixture are illustrated by the diagram shown in Fig. 1. This figure indicates that there are several pathways resulting in the formation of KrF*. When pure electron-beam excitation is used the dominant mechanisms are two and three-body positive and negative ion recombination, the positive ions having been produced by ionization initiated by the high energy primary electrons in the beam, and the negative ions by dissociative attachment reactions involving low energy electrons and F_2. Reactions between F_2 and rare-gas metastable atoms produced by low energy electron impact are the primary source of rare gas-monohalide molecules in electron-beam controlled discharges. Recombination and metastable reactions may make comparable contributions to rare-gas halide formation in fast pulse, self-sustained laser discharges, depending on specific circumstances. Of course there are numerous reactions which tend to interrupt the chain of events illustrated in Fig. 1. Nonetheless the energy utilization efficiency associated with rare-gas monohalide molecule formation is typically in excess of 20 percent for conditions representative of both electron-beam excited and electron-beam controlled lasers.[1] However, electron-beam

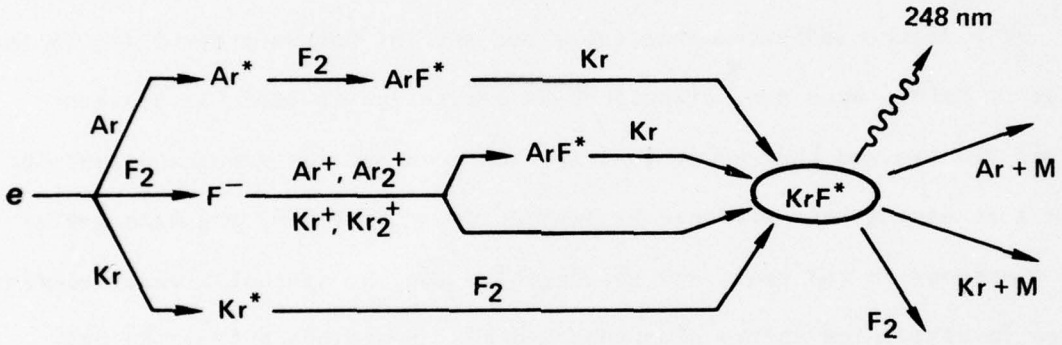

Fig. 1. Illustration of the primary reactions contributing to KrF* formation and loss in an electrically excited Ar-Kr-F_2 mixture at nominally atmospheric pressure.

78-06-7-6

controlled-discharge excited lasers, for which most of the energy is provided by the discharge, have greater potential for scaling to high average power than lasers excited by an electron-beam alone.

Figure 1 indicates that there are several processes contributing to the loss of KrF*; these are also found to be of comparable importance for typical conditions. In subsequent paragraphs specific details of the reactions indicatedin Fig. 1 will be discussed with emphasis directed toward factors of importance in discharge excited KrF* lasers.

B. Electron Collision Processes

Electron-Neutral Energy Transfer

A fundamental factor contributing to the high efficiency characteristic of discharge excited rare-gas halide lasers is the efficient production of rare-gas metastable atoms for conditions readily attainable experimentally. Shown in Fig. 2 are the computed variations of the processes dominating electron-atom (molecule) energy transfer for conditions typical of an electron-beam controlled KrF* laser. For E/n values[a] greater than approximately 1.0×10^{-16} Vcm^2, for which the mean electron energy[b] is about 3.25 eV for the mixture indicated, the combined argon and krypton metastable production efficiencies exceeds 50 percent, and reach 70 percent for higher E/n values. Examination of Fig. 2 indicates that the contributions to the undesirable loss of electron energy due to elastic collisions with atoms, excitation of metastable atoms to higher states, and F_2 dissociation

---

a) E/n is the ratio of electric field intensity to total neutral number density.

b) Mean electron energy as used here is defined as 2/3 the average energy.

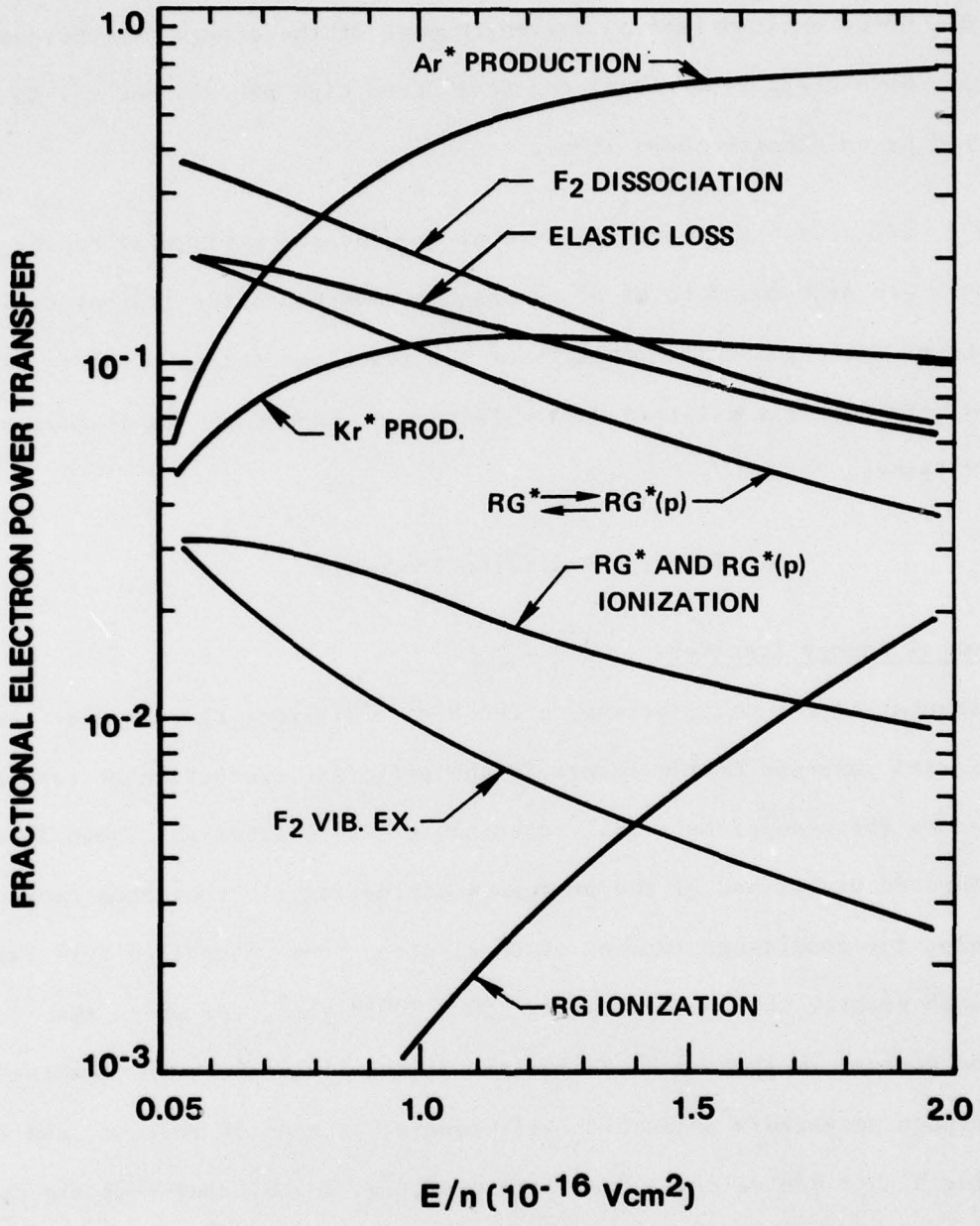

Fig. 2 Fractional contributions to electron-neutral power transfer in an Ar-Kr-F_2 mixture having the proportions 0.945-0.05-0.005. For this example the fractional ionization, fractional metastable concentration and fractional concentration of rare gas p state atoms were 10^{-6}, 10^{-5} and 10^{-6}, respectively. The notation RG refers to the combined effect of Ar and Kr.

78-06-7-3

are found to be of comparable importance for the conditions of this example. However, it will be shown that the net effect of electron excitation and de-excitation of rare-gas atoms between their metastable and p states is highly variable, depending on the concentration of metastable atoms. For fractional metastable concentrations greater than the 10^{-5} value typical of this example the power loss accompanying this process increases significantly.[6,10] Although the energy loss associated with ionization of excited states and of ground state atoms is small, these processes make very important contributions to the production of electrons in electron-beam controlled discharges.

Even though the cross-sections for electron excitation of F_2 vibrational levels are relatively large ($\sim 10^{-17}$ cm^2)[11], vibrational excitation does not appear to be an important energy loss process because the energy loss per collision is small (~ 0.1 eV).[12] Although there are no electron cross-section data for F_2 electronic excitation, this process may be important because the electron energy loss will be several electron-volts. Additionally, there are numerous F_2 electronic states in the 3 to 10 eV range which are repulsive[13] and which would therefore result in F_2 dissociation when excited. In this energy range there are likely to be excited states of the F_2^- ion which lie above dissociating states of F_2 in the vicinity of the F_2 equilibrium internuclear separation. Thus, for electron energies of a few electron volts F_2 electronic excitation may be enhanced by resonance processes as is the case with dissociative attachment.[14-16] In order to reasonably account for the effect of F_2 electronic excitation indirect experimental evidence of F_2 dissociation has been analyzed, from which an effective e-F_2 dissociation cross section has been obtained.[12] Based on

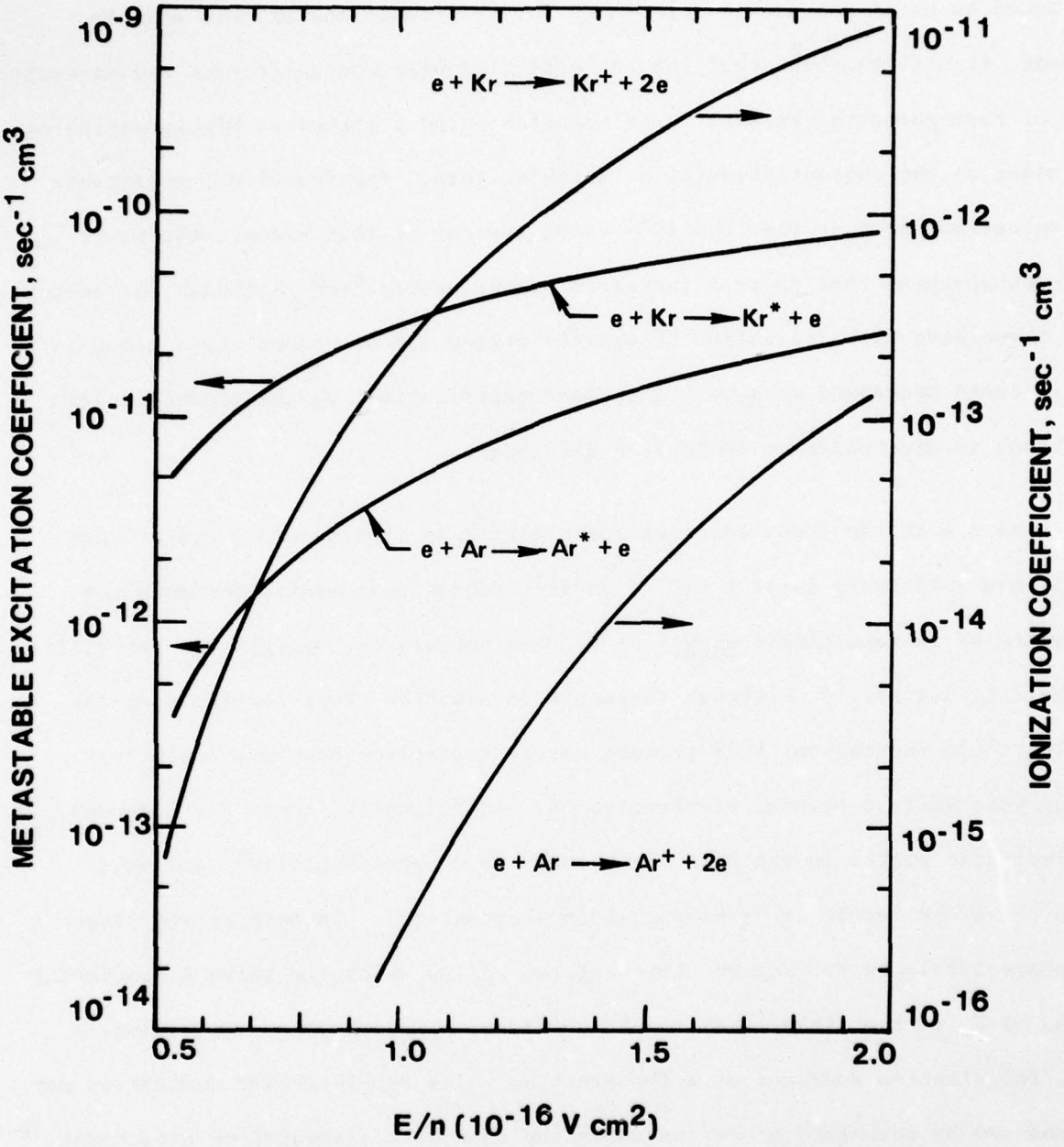

Fig. 3 E/n variation of the metastable excitation and ionization rate coefficients for ground state Ar and Kr corresponding to the conditions of Fig. 2.

78-06-7-1

this provisional cross-section the data of Fig. 2 show that electron energy loss accompanying direct dissociation by electrons is likely to be substantial for halogen molecule concentrations typical of rare-gas halide lasers. In addition, the contribution of this process to F_2 dissociation will also be shown to be significant.

Electron Rate Coefficients

Presented in Fig. 3 is the E/n variation of the electron rate coefficients for metastable excitation and ionization from the ground state corresponding to the conditions of Fig. 2. These data were generated using available cross-section information.[17,18] With a mean electron energy much lower than the threshold for excitation, only those electrons in the high energy region of the electron energy distribution participate in the metastable production and ionization processes. This accounts for the characteristically strong dependence of the rate coefficients for these processes on E/n (i.e. mean electron energy). The higher rate coefficients for Kr reflect the fact that the energy thresholds for excitation and ionization of krypton are lower than the respective thresholds for argon.

In most if not all electronically excited excimer lasers the fractional ionization exceeds 10^{-6} and the fractional metastable concentration exceeds 10^{-5}. For these circumstances electron-electron[19,20] collisions and electron collisions with metastable atoms[6] exert an important influence on the electron energy distribution, the former tending to increase the number of high energy electrons and the latter resulting in a decrease in their number. Those electron rate coefficients which are particularly sensitive to the high energy region of the distribution are most affected by such changes. Thus, in addition to their strong dependence on E/n, the rate coefficients for electronic excitation and ionization of ground state rare gas atoms exhibit a significant dependence on degree of ionization and on fractional metastable

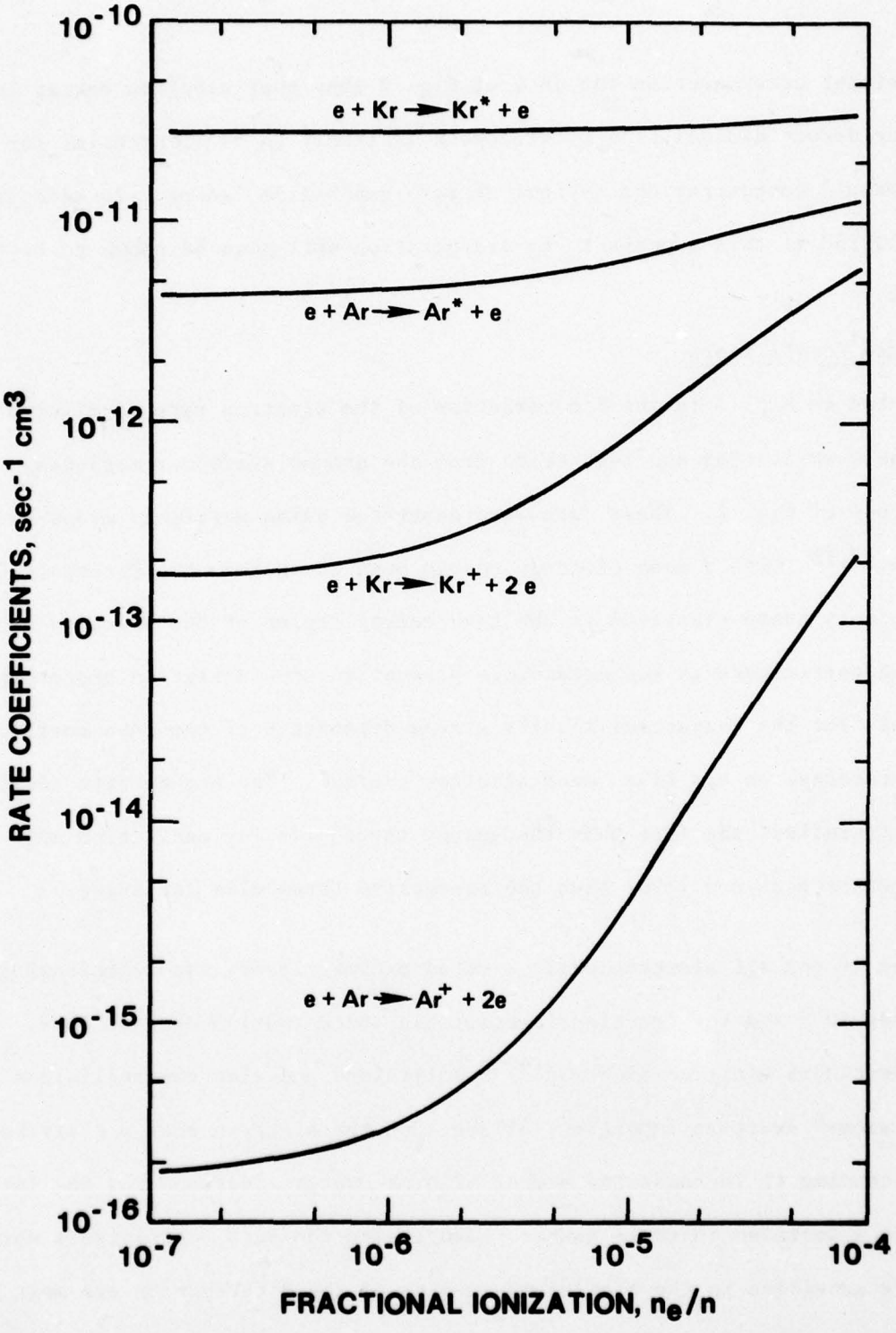

Fig. 4 Variation of Ar and Kr rate coefficients for metastable production and ionization with fractional ionization for an E/n value of 1.0×10^{-16} Vcm^2. The fractional concentrations of metastable and p state atoms were fixed at 10^{-5} and 10^{-6}, respectively.

78-06-7-17

concentration. The results presented in Figs. 4 and 5 illustrate this effect for representive KrF* laser conditions. The influence of electron-electron collisions is particularly striking (Fig. 4), resulting in nearly a two order-of-magnitude increase in the rate coefficient for Kr ionization and a three order-of-magnitude increase for Ar as the fractional ionization increases in the 10^{-6} to 10^{-4} range typical of rare-gas halide discharges.

Figure 5 indicates that variations in rare gas excitation and ionization rates caused by cooling of the electron energy distribution due to excitation of metastable atoms to higher levels are also significant. Of more importance is the fact that since fractional ionization and fraction metastable concentration generally increase together, the effects illustrated in Figs. 4 and 5 tend to be partially offsetting. In addition, the variation shown in these figures for a fixed E/n value of 1.0×10^{-16} Vcm^2 becomes greater as E/n is reduced below this level and are smaller for higher E/n values. Thus, in modeling rare-gas halide laser discharges it is necessary to evaluate rate coefficients for ionization and excitation from the ground state using self-consistent combinations of E/n, degree of ionization, and metastable fraction.

Presented in Fig. 6 are the E/n variations of the rate coefficients for Ar and Kr excitation and de-excitation between the grouped metastable and p states, calculated using available cross-section data.[21] Rate coefficients for ionization from both the metastable and p states are also shown.[22,23] These data exhibit a weak dependence on E/n reflecting the fact that the energy thresholds for the processes involved are comparable to (or less than) the mean electron-

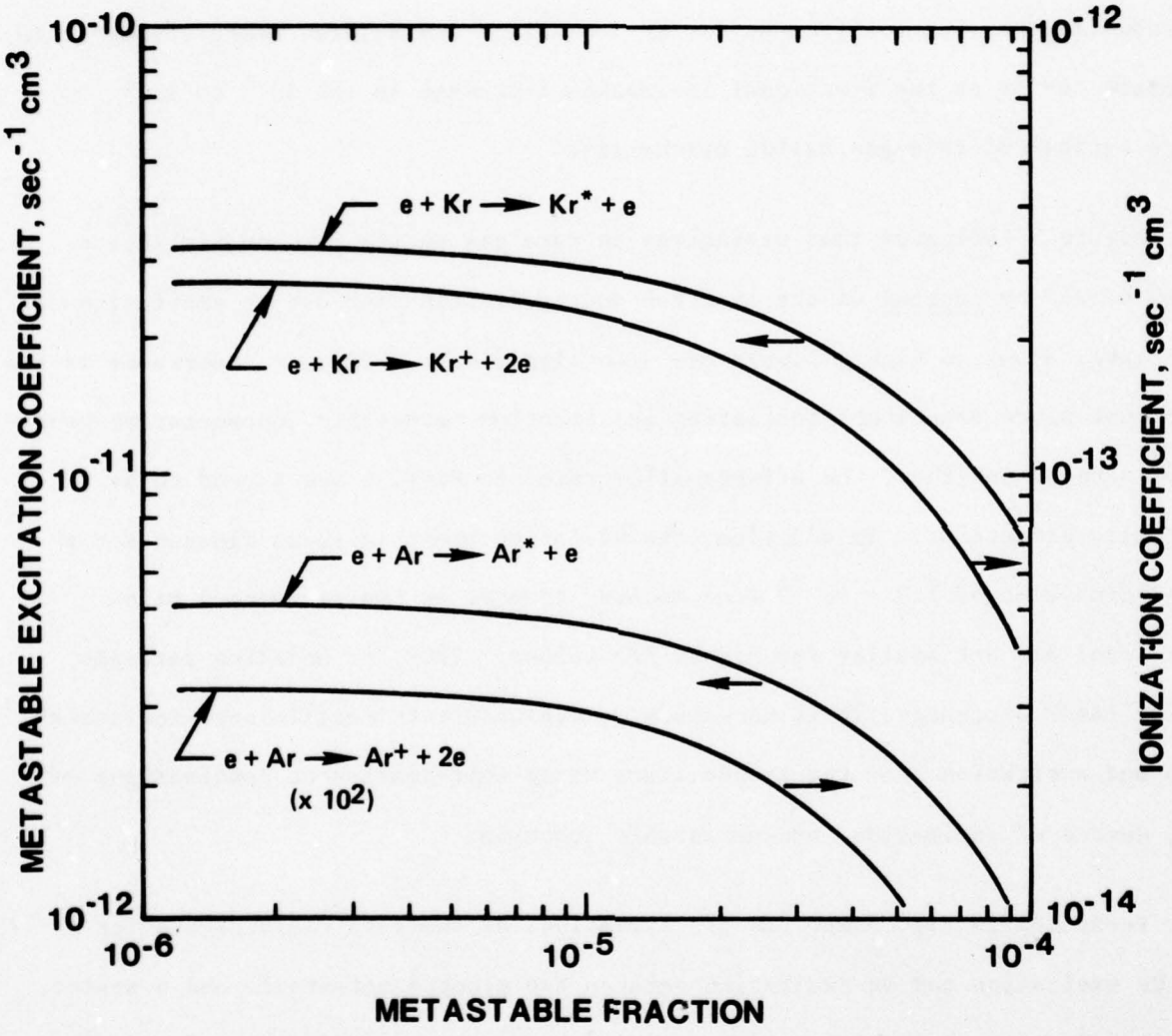

Fig. 5 Variation of Ar and Kr rate coefficients for metastable production and ionization with metastable fraction for an E/n value of 1.0×10^{-16} Vcm^2 and a fractional ionization of 10^{-6}. The fractional p state concentration was increased in proportion to the metastable fraction so that the p state : metastable ratio was always 0.1.

78-06-7-19

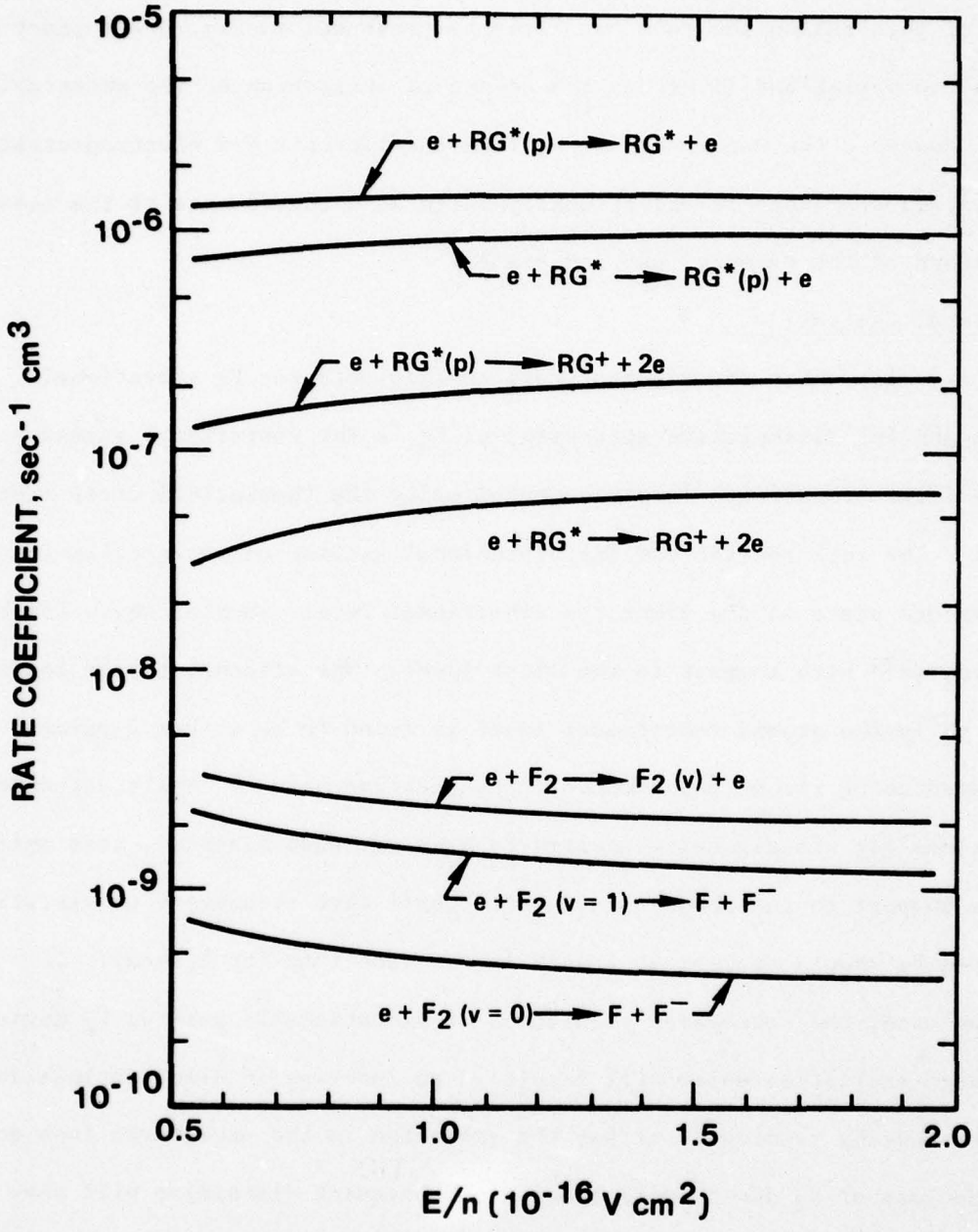

Fig. 6 F/n variation of electron rate coefficients for excitation, de-excitation and ionization of rare gas p state atoms, along with the rate coefficients for metastable ionization, F_2 dissociative attachment and F_2 vibrational excitation. The rate coefficients for these processes exhibit very little change in response to variations in fractional ionization or excited state concentration. The notation RG refers to either Ar or Kr.

78-06-7-2

energy. For this reason the rate coefficients presented in Fig. 6 are practically insensitive to variations in either the degree of ionization or the metastable fraction. However, the magnitude of the rate coefficients for electron-excited state collision processes is exceptionally large as a consequence of the alkali-like structure of the rare-gas excited states.[21].

F_2 Vibrational Excitation

Figure 6 also shows the electron rate coefficients for F_2 vibrational excitation and for dissociative attachment of F_2 in the vibrational ground state and in the first vibrational level, computed using the theoretical cross sections of Ref. 11. The rate coefficient for vibrational excitation reflects excitation from the ground state to the first ten vibrational levels each of which has been energy weighted[24] with respect to the first level. The attachment rate coefficient for F_2 in the ground vibrational level is found to be within 5 percent of that computed using recent experimental cross section data.[16] While attachment cross sections for vibrationally excited F_2 have not been measured, this agreement lends support to the theoretical prediction[11] that attachment to vibrationally excited F_2 should proceed at a much faster rate than for $F_2(v=o)$. If such is the case, the increasing population of vibrationally excited F_2 during the discharge excitation pulse will result in an increase in electron loss due to attachment, thereby tending to offset the reduction in the attachment loss accompanying the loss of F_2 due to dissociation. Subsequent discussion will show that such an effect could influence the onset of plasma instability.

C. Excited State Processes

In addition to efficient rare gas metastable production, efficient rare-gas monohalide formation requires that reactions leading to the formation of KrF* dominate over competing metastable quenching processes. Thus, reactions between rare-gas metastable atoms and the halogen "fuel" molecule must be the dominant metastable loss process; and the branching ratio for the formation of the desired rare-gas monohalide molecule must be near unity. Setser and co-workers[25] have conducted extensive investigations of rare-gas metastable atom quenching and have found that practically all halogenated molecules have large rate constants. Moreover, diatomic halogens such as F_2 have near unity branching ratio for rare-gas monohalide formation. Thus, energy efficient formation of rare-gas-monohalide molecules is usually assured in discharges in which rare-gas metastables are produced efficiently, and in which an appropriate halogen fuel molecule is present.

With a stimulated emission cross section in the 1 to 5 x 10^{-16} cm^2 range,[1] maintenance of optimum gain requires a rare-gas monohalide density of about 10^{14} cm^{-3}, a relatively high excited state concentration even for an atmospheric pressure glow discharge. Thus, knowledge of rare-gas halide loss mechanisms under various conditions is particularly important. The dominant rare-gas halide quenching processes have been identified by Rokni, Jacob and Managano whose detailed analysis and interpretation is presented elsewhere.[5] Certain of their results relevant to KrF* lasers are summarized in Table I along with other related data.[26-30] It is worth pointing out that each of the major constituents in the gas mixture collisionally quenches[5] KrF* (Fig. 1, Table I). Additionally, with a radiative lifetime less than 10 nsec spontaneous decay of the rare-gas monohalide laser molecule is always important for the conditions of interest.

TABLE I

RARE GAS AND RARE GAS-HALIDE NEUTRAL REACTIONS AND RATE COEFFICIENTS FOR KrF* LASERS

Reaction	Rate Coefficient[a)]	Reference
$Ar^* + Kr \rightarrow Kr^*(p) + Ar$	5.6 (-12)	26
$Ar^* + F_2 \rightarrow ArF^* + F$	7.5 (-10)	5
$Kr^* + F_2 \rightarrow KrF^* + F$	7.8 (-10)	5
$Ar^*(p) + Ar \rightarrow Ar^* + Ar$	2-6 (-11)	30
$Kr^*(p) + Ar \rightarrow Kr^* + Ar$	2-6 (-11)	estimated (see 30)
$ArF^* + Kr \rightarrow KrF^* + Ar$	1.6 (-9)	5
$ArF^* + Ar + M \rightarrow Ar_2F^* + M$	4.0 (-31)	5
$KrF^* + Kr + M \rightarrow Kr_2F^* + M$	6.5 (-31)	5
$KrF^* + 2Ar \rightarrow$ products	7.0 (-32)	5
$ArF^* + F_2 \rightarrow$ products	1.9 (-9)	5
$KrF^* + F_2 \rightarrow$ products	7.8 (-10)	5
$KrF^* \rightarrow Kr + F + h\nu$ (248 nm)	9 (-9)	27
$ArF^* \rightarrow Ar + F + h\nu$ (193 nm)	$\sim$ 4 (-9)	29
$Kr_2F^* \rightarrow 2Kr + F + h\nu$ (400 nm)	181 (-9)	28
$Ar_2F^* \rightarrow 2Ar + F + h\nu$ (290 nm)	132 (-9)	29

a) Units: two-body processes, $sec^{-1}\ cm^3$; three-body processes, $sec^{-1}\ cm^6$; radiative processes, sec. The number in ( ) refers to the exponent of ten.

Quenching of Rare-Gas P State Atoms by Neutral Collisions

Figure 6 shows that the rate coefficient for electron impact excitation of rare-gas metastable atoms to the higher lying manifold of p states[21] is very large. Indeed, for the conditions encountered in rare-gas halide lasers this process can compete with the desired metastable-F_2 rare-gas monohalide formation channel. Thus, the significance of p state excitation from the metastable state depends on what happens to the p-state atoms after they are produced. For this reason a knowledge of p-state quenching processes is particularly important. Recently Change and Setser[30] reported rate coefficients for collisional quenching of Ar p-state atoms by argon at room temperature (Table I). Their results show that metastable production as a result of p-state quenching by ground state atoms will be very fast for pressure typical of rare-gas halide lasers. Such p-state-metastable transitions can be explained[30] in terms of a curve crossing mechanism among the Ar_2^* repulsive states which then dissociate, e.g., $Ar^*(p) + Ar \rightarrow Ar_2^* \rightarrow Ar^* + Ar$. Subsequent discussion will show that this process can dominate p-state atom quenching in rare-gas halide lasers thereby exerting an important influence on both rare-gas halide formation efficiency and plasma stability.

III. LASER DISCHARGE ANALYSIS

A. Temporal Variations

Plasma Modeling

Analysis of plasma properties in pulsed rare gas-halide lasers requires modeling of the time dependent variation of electron, ion and excited state processes for conditions typical of the excitation scheme of interest,[1,6,7] In the present work emphasis has been placed on electron-beam controlled laser discharges operating under conditions similar to those described in Ref. 31. For the most part the modeling procedures used are similar to those typically employed in such analyses.[6,7] The principle electron and excited state reactions and rate coefficients used in the present analysis have been discussed in the preceding section and are presented in Figs. 3-6 and in Table I. The dependence of electron-atom rate coefficients on variations in E/n, fractional ionization and metastable fraction was accounted for by solving the Boltzmann equation[19,24] in order to generate a matrix of data similar to those presented in Figs. 3-5. On the basis of the data so obtained rate coefficients for excitation and ionization from the ground state were represented analytically by an expression of the form,

$$k(E/n, \alpha, \delta) \equiv k_0(E/n) f(E/n, \alpha) g(E/n, \delta) \ ,$$

where k is the rate coefficient for a particular process, α is the fractional ionization, δ is the metastable fraction, and f and g are E/n dependent analytic

functions reflecting the numerically determined variations in k with changes in α and δ (Figs. 4 and 5). Thus, k_o was determined by specifying an E/n value in the range of interest. The rate coefficients, $k(E/n, \alpha, \delta)$ were then computed as a function of time using self-consistent values of α and δ.

Species Concentrations

Figure 7 presents the computed temporal variation of selected species for representative experimental conditions.[31] In this example the external ionization source was increased as a function of time in order to simulate the increase in e-beam current density typical of pulsed, cold-cathode e-gun operation.[31] For these conditions plasma properties reach quasi-steady values in a time less than 0.1 μsec. However, Fig. 7 shows that significant changes occur on a longer time scale because of the combined influence of the increasing e-beam ionization rate and F_2 dissociation, particularly the latter. Indeed, for this example F_2 dissociation exceeds 25 percent after about 0.6 μsec. The results presented in this figure show that the fractional ionization ($\alpha = n_e/n$) and metastable fraction ($\delta = n^*/n$) are approximately 4×10^{-6} and 10^{-5}, respectively, values for which electron rate coefficients are affected by collisions with other electrons and with metastable atoms (Figs. 4 and 5). In addition, Fig. 7 shows that after a few tenths of a μsec the concentrations of vibrationally excited F_2 and of F atoms reach levels corresponding to about one-tenth the initial F_2 density.

The computed populations of all excited species considered in the present analysis are presented in Fig. 8 for a time 0.4 μsec after discharge initiation. This figure shows that the primary excited species are the rare gas metastables, Ar* and Kr*, and the krypton-fluorides KrF* and Kr_2F^*, each having concentrations

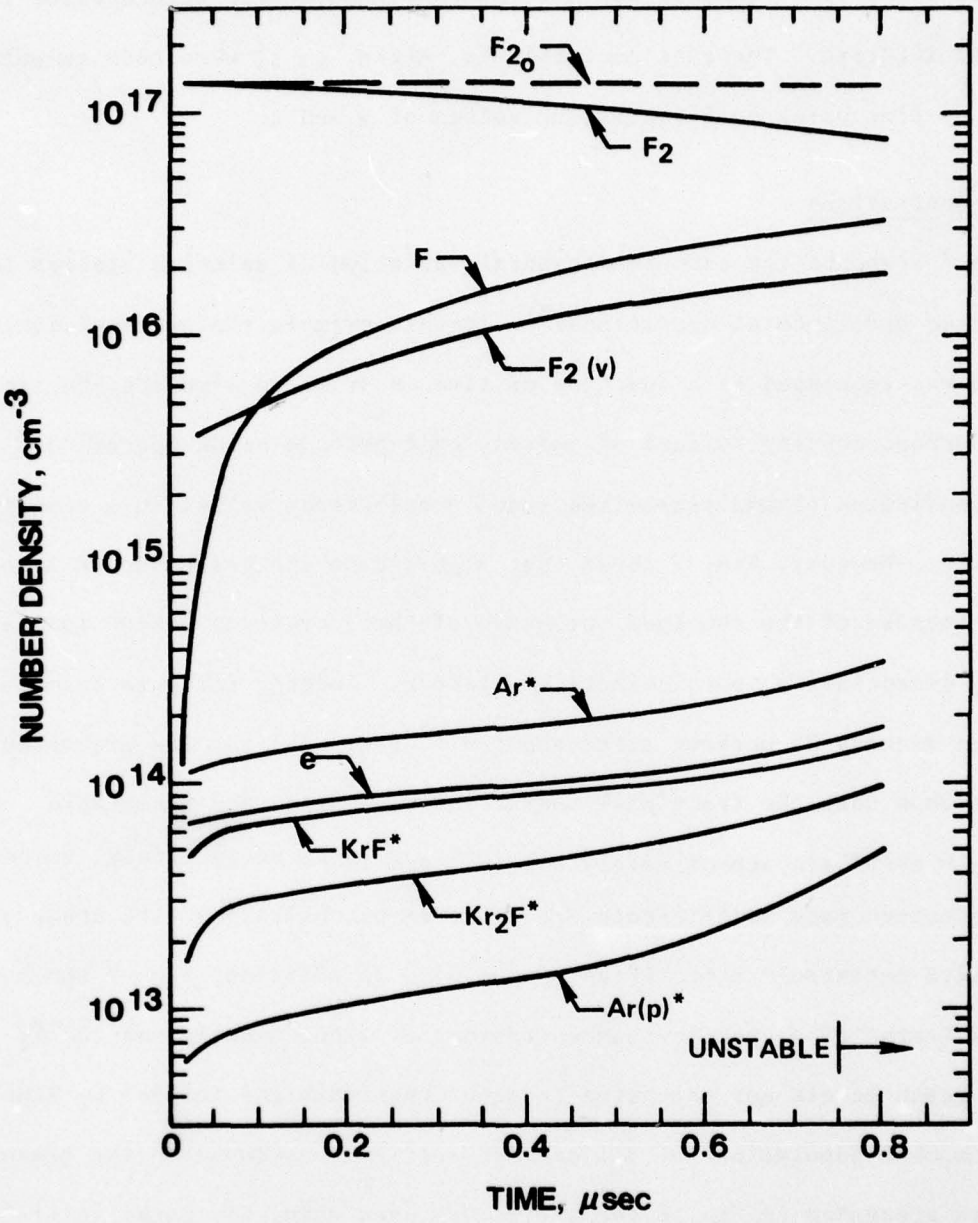

Fig. 7 Temporal variation of selected species in an e-beam controlled KrF* laser discharge at a pressure of one atm; Ar-Kr-F_2 (0.945-0.05-0.005). For this example the E/n value was 1.2×10^{-16} Vcm^2; and the temporal variation of the e-beam ionization rate was $160 + 8 \times 10^7 t$ sec^{-1} resulting in a 50 percent increase in the electron production rate after 1 μsec.

78-06-7-7

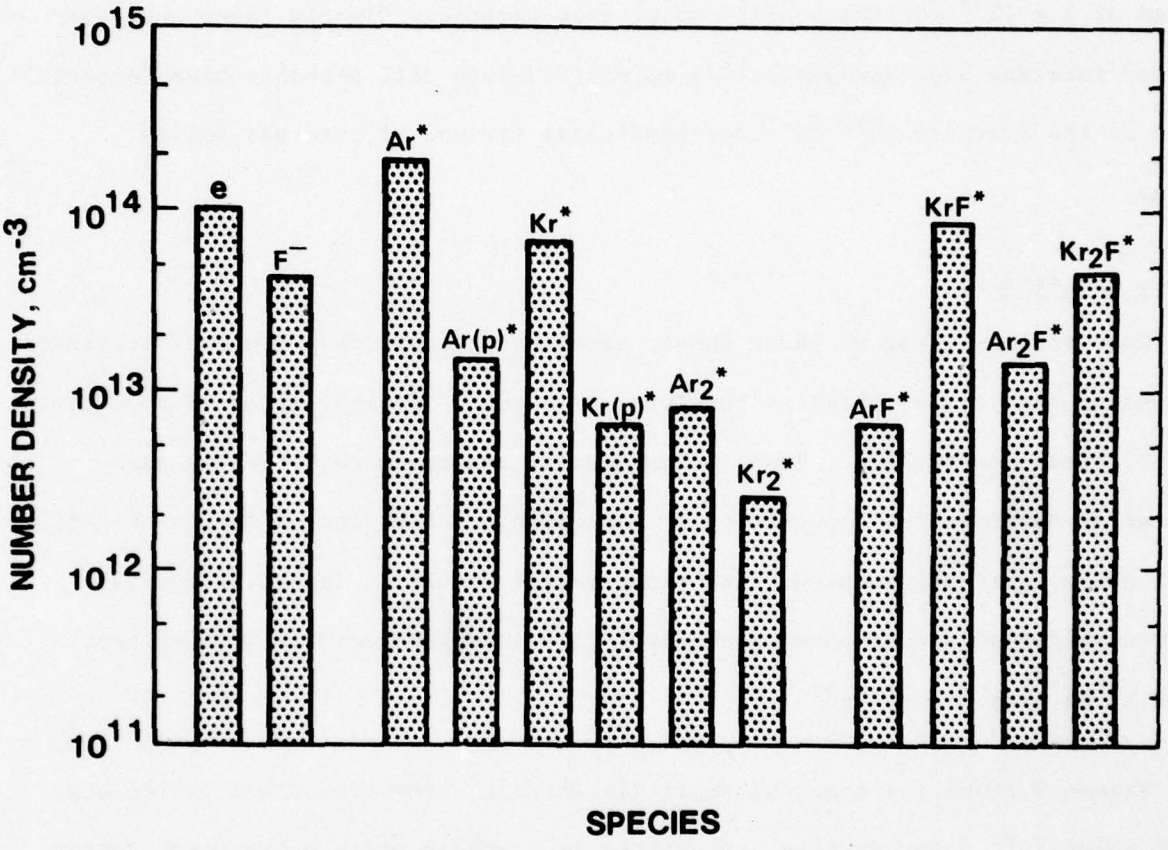

Fig. 8 Particle concentrations corresponding to the conditions of Fig. 7 at a time 0.4 μsec after discharge initiation.

78-06-7-10

of approximately 10^{14} cm^{-3}. Other excited species have number densities in the $2 \times 10^{12} - 2 \times 10^{13}$ cm^{-3} range, with the total excited state fraction in excess of 2×10^{-5} for the conditions of this example. Clearly there are other excited rare gas and rare-gas halide molecules which will probably have concentrations on the order of 10^{12} cm^{-3} for conditions typical of rare-gas halide lasers.

Medium Properties

Numerical modeling of laser characteristics begins with a study of microscopic processes, analysis of which is the primary source of insight required to optimize and/or improve conditions. However, an equally important objective of such studies is quantitative computation of macroscopic properties of the laser medium which can be directly compared with experimental results. Indeed, comparison between predicted and measured rare-gas halide laser characteristics has been found to be very good.[1,7,31]

Figure 9 shows the computed small signal gain, KrF* production efficiency, total volumetric power density, and discharge : e-beam power enhancement factor corresponding to the conditions of Figs. 7 and 8. The KrF* production efficiency (η) as used here includes the quantum efficiency and as such represents the fraction of the total power potentially available for conversion to optical power. The enhancement factor (EF) is simply the ratio of the discharge power to that supplied by the e-beam. The data of this figure illustrate the high gain and remarkable rare-gas monohalide production efficiency characteristic of rare-gas halide lasers, KrF* in particular. Note, however, that although the power density is dominated by the discharge contribution (EF > 1), the enhancement factor is

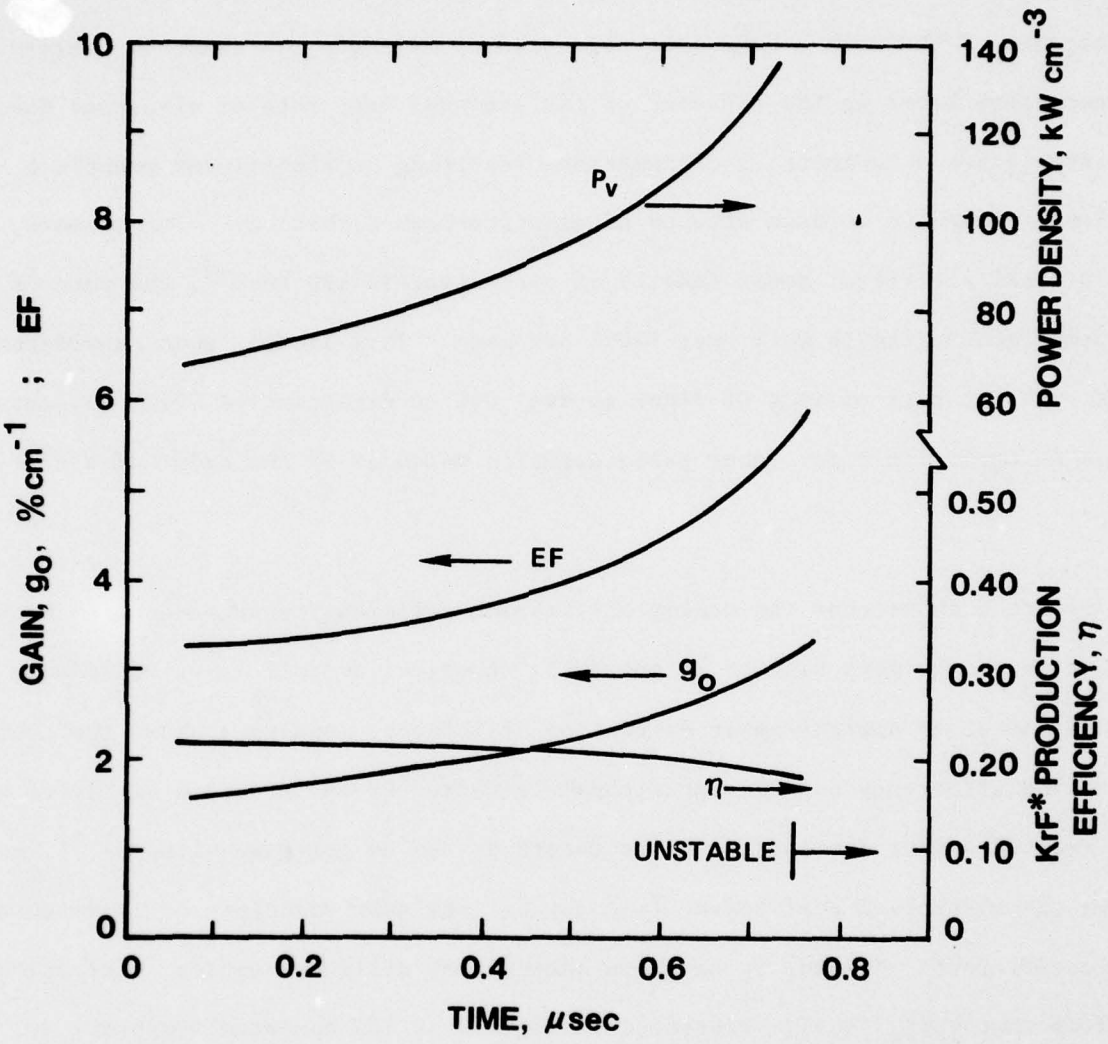

Fig. 9 Temporal variation of total electrical power density (P_v), discharge : e-beam power enchancement factor (EF), small signal gain (g_o), and KrF* production efficiency (η) for the conditions of Fig. 7.

78-06-7-20

very much lower than that typical of ir molecular lasers.[9] This is a direct consequence of the high e-beam power required to maintain the electron density at the necessary level in the presence of the enormous loss rate of electrons due to F_2 dissociative attachment, a circumstance resulting in significant practical problems related to certain aspects of electron-beam technology. Furthermore, with a total electrical power density of approximately 100 $kWcm^{-3}$, the rate of gas temperature rise is well over 100°K per μsec. This factor, when considered along with the rate of loss of fluorine fuel due to dissociation (Fig. 7), establishes an upper limit for laser pulse duration which is on the order of a few μsec.

Figure 9 shows that the energy utilization efficiency associated with KrF* production can be very high (≈ 20 percent). However, overall laser efficiency is also dependent on optical power extraction efficiency. Analysis shows that optical extraction efficiency can be significantly affected by the presence of electronically excited and/or ion species which absorb at the uv laser wavelength[1,32], even though the absorption coefficient (γ_o) may be less than one-tenth as large as the gain coefficient. Indeed, it has been shown[1] that efficient optical extraction requires that $\gamma_o/g_o < 0.1$. Presented in Fig. 10 is the computed temporal variation of the total absorption coefficient at the KrF* laser wavelength (248 nm) corresponding to the conditions of Fig. 7. Also shown are the individual contributions from known absorbing species, computed on the basis of reported cross-section data.[32] For the conditions of this example photodissociation of F_2 is obviously the dominant laser absorption process. However, the concentrations of ionic and excited species are subject to much greater variation than the F_2 density, and their

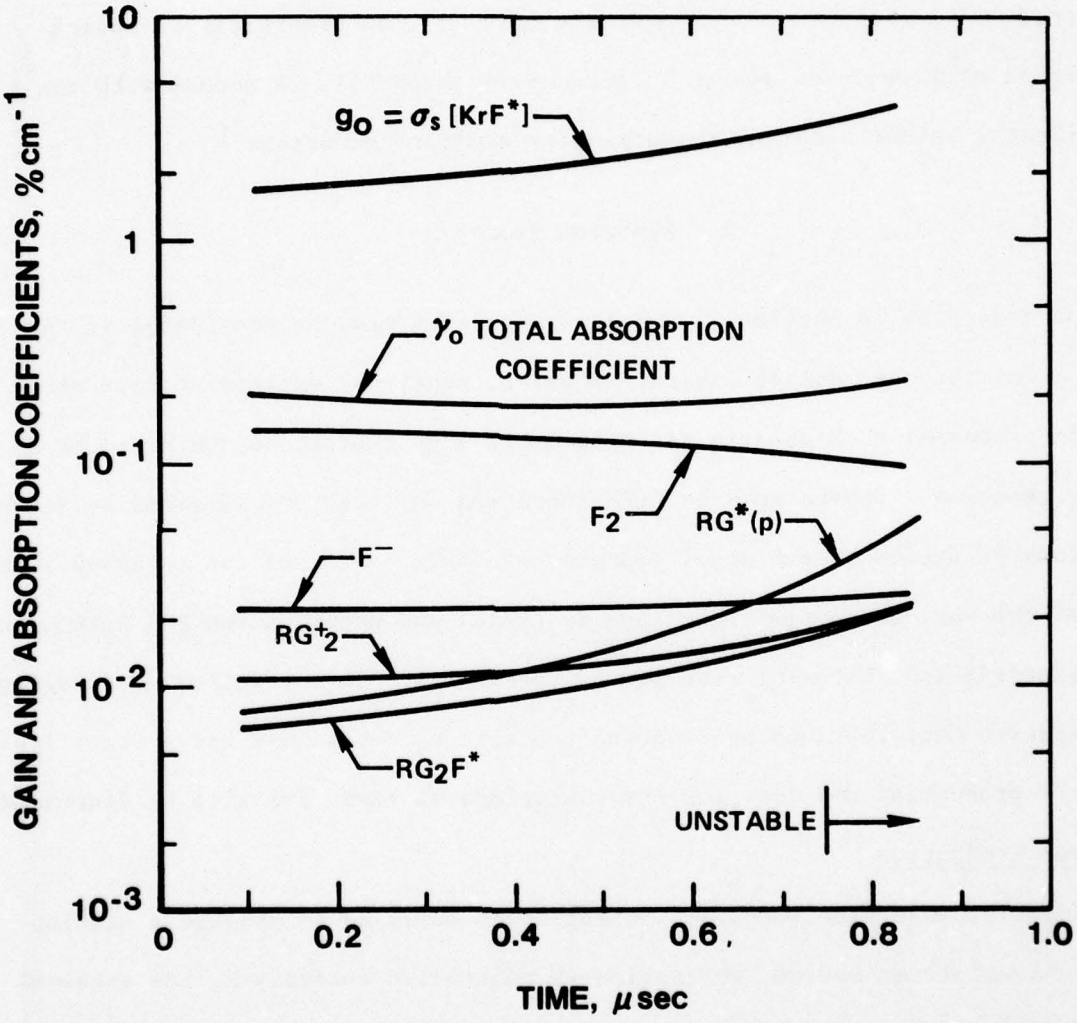

Fig. 10 Temporal variation of small signal gain and absorption coefficients for the conditions of Fig. 7. The KrF* stimulated emission cross-section used was 2.4×10^{-16} Vcm^2; and the absorption cross sections used for the species indicated were those reported in Ref. 32. In this figure the notation RG refers to the combined effect of Ar and Kr.

78-06-7-11

combined influence is very significant as indicated in Fig. 10. Analysis of optical extraction efficiency for the conditions of this figure yields a value of about 45 percent for an active medium length of one-meter. When combined with a KrF* production efficiency of 20 percent (Fig. 9), an electrical-to-optical conversion efficiency of almost 10 percent is indicated, in accord with the highest experimental values attained to date under similar conditions.[1]

B. Dominant Processes

As indicated in Section II numerous processes must be considered in the analysis of rare-gas halide lasers. However, numerical experimentation shows that certain processes such as rare gas metastable loss tend to be dominated by a single reaction. Others such as KrF* formation and loss are affected by several reactions of approximately equal importance. Examination of the relative importance of the various coupled reactions is useful and provides insight helpful to understanding and improving rare-gas halide lasers. In the following paragraphs the relative contributions to electron production, metastable and p state loss, and KrF* production and loss for the conditions of Figs. 7-9 will be discussed.

Electron Production

Ideally, when electron-beam ionization is employed to provide a stable, large volume plasma medium, ionization is controlled entirely by the external ionization source, effectively decoupling electron production from other plasma properties. Such is the case in ir molecular lasers[9], for example, in which the mean electron energy required for efficient vibrational excitation is much less than that for which electronic excitation and ionization become significant.

However, in rare-gas halide lasers (and other excimer lasers as well) the mean electron energy required is several electron volts and the density of electronically excited species is high.[9] Given these circumstances along with the alkali-like structure of rare gas metastables, significant ionization by low energy plasma electrons is usually unavoidable even when an external ionization source is used.

Figure 11 compares the various fractional contributions to electron production in a KrF* laser discharge operating under the conditions of Fig. 7. These results show that although ionization by the high energy e-beam is dominant, low energy electron impact ionization of rare gas metastable atoms provides almost 20 percent of the ionization, a contribution which increases significantly with time. Indeed, even ionization of argon and krypton p states is important for the conditions of this example. The non-negligible contribution of ground state ionization is a direct reflection of the increase in the ionization rate coefficient caused by electron-electron collisions.

The relative contributions to the ionization process as indicated by Fig. 11 are typical of the e-beam controlled rare-gas halide lasers that have been oprerated to date.[1,31,33-35] On the basis of these results it is apparent that such discharges are actually of a hybrid nature in which substantial contributions to ionization are made by both high energy beam electrons and by plasma electrons.

Metastable and P State Loss Processes

In e-beam controlled rare-gas halide discharges production of rare gas metastable atoms is dominated by a single process, electron impact excitation of ground state atoms. However, there are several reactions by which metastable atoms are

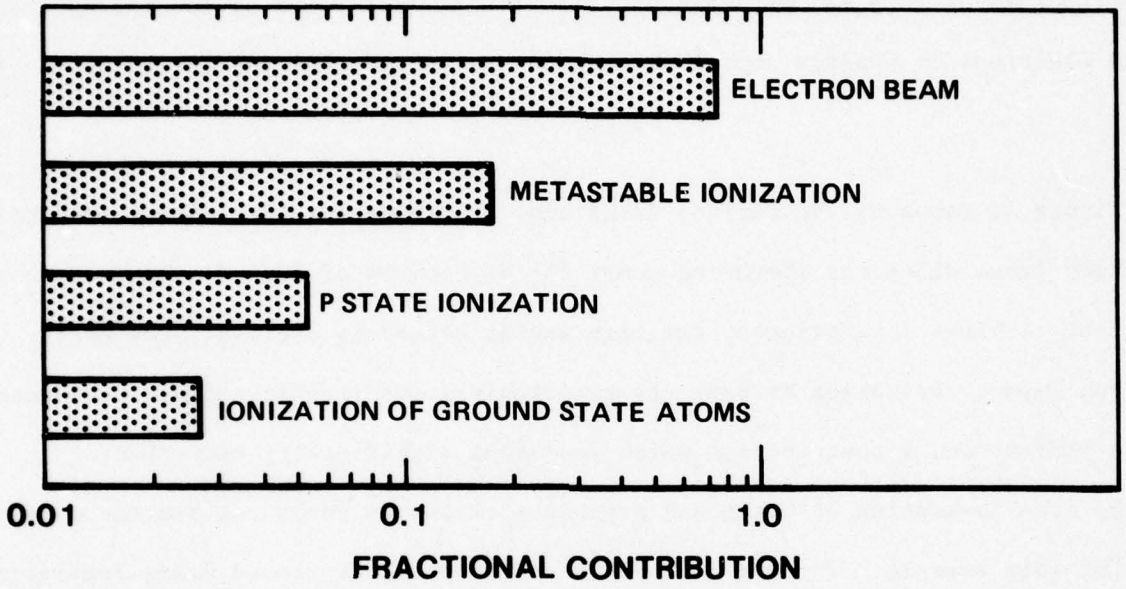

Fig. 11 Fractional contributions to electron production in an e-beam controlled KrF* laser discharge for the conditions of Fig. 7. These results, and those presented in Figs. 12, 13 and 15-17, refer to the time 0.4 μsec after discharge initiation and are representative of conditions in the 0.2 to 0.6 μsec time range.

78-06-7-8

lost. Figure 12 presents a comparison of the Ar* loss processes for the conditions of present interest. The effect of coupling between the metastable and p states has been grouped as a single process as indicated. Thus, Ar* $\rightleftarrows$ Ar*(p) represents the net effect of electron excitation of the p states from the metastable states, and transitions back to the metastable states caused by both electron and neutral collisions and by radiative decay. This figure vividly illustrates the dominance of the desired metastable-halogen reaction[25] and in part explains why the KrF* laser is so attractive. Although such selectivity is a requirement for efficient KrF* formation, a consequence of the dominance of the RG*-F_2 reaction is that the metastable concentration is particularly sensitive to the loss of F_2 due to dissociation. Since metastable ionization makes a significant contribution to electron production (Fig. 11), the increased metastable concentration accompanying dissociative loss of F_2 has a particularly serious effect on plasma stability, a topic which is discussed in a subsequent section.

For the reasons discussed in Section II knowledge of the processes by which rare gas p state atoms are lost is of considerable importance. There are numerous processes resulting in the loss of p-state atoms including: electron superelastic collisions by which p-state atoms are converted back to metastable states with no net loss of electron energy, halogen reactions,[a] quenching by neutrals which also results in metastable production,[30] electron excitation and ionization, and spontaneous radiative transitions back to the metastable states. Presented in

---

(a) In this analysis it has been assumed that p-state-F_2 reactions result in RGF* formation and proceed at rate equal to that of the corresponding metastable reaction.

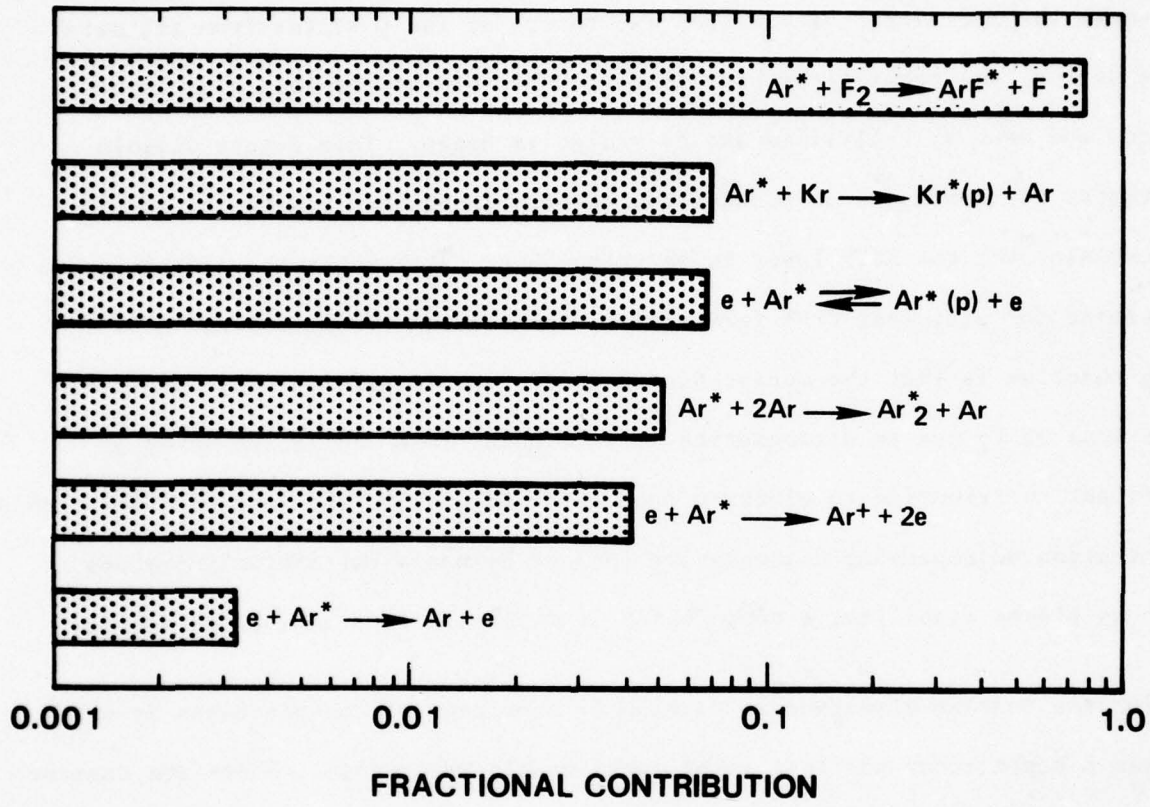

Fig. 12 Fractional contribution to argon metastable loss in an e-beam controlled KrF* laser discharge for the conditions of Fig.7.

78-06-7-12

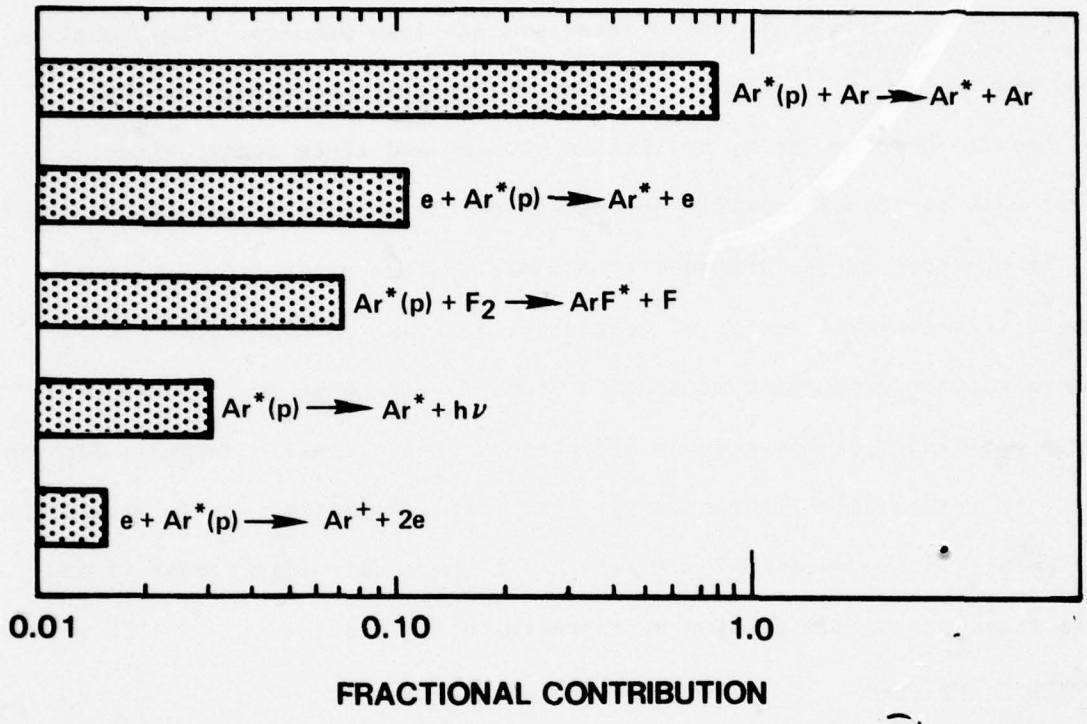

Fig. 13 Fractional contributions to the loss of argon p state atoms in an e-beam controlled KrF* laser discharge for the conditions of Fig. 7.

78-06-7-15

Fig. 13 are the relative contributions of these processes to the loss of argon p-state atoms. These results show that neutral quenching of p-state atoms by ground state rare-gas atoms is the dominant p-state loss process. Thus, p-state atoms produced by way of electron collisions with metastable atoms are rapidly converted back to metastables by collisions with ground state atoms, with the result that this process has little net effect on the density of metastable atoms. However, the electron energy expended to produce p-state atoms from metastables is converted to translational energy of neutrals. As long as the electron energy loss associated with production of p-state atoms is not large the laser energy utilization efficiency is not greatly affected by this process. However, Fig. 14 shows that the fractional electron energy loss associated with p-state excitation depends directly on the metastable density and becomes very significant if the metastable fraction exceeds a value of approximately 3×10^{-5}.

KrF* Formation and Loss

The mechanisms responsible for rare-gas halide formation and loss have been the subject of extensive experimentation and analysis.[1,5,25,27,28] As a result the reactions of primary importance have been identified and a generally complete set of rate data are available for use in analyses such as that described herein. Figures 15 and 16 present a comparison of the relative importance of KrF* production and loss for the conditions of Fig. 7. For the conditions of this example the ArF*-Kr displacement reaction[5] dominates the formation of KrF*. Examination of Figs. 2, 12 and 15 reveal the direct, efficient channel of energy from the electrons to Ar* to ArF*, and finally to KrF*. For typical conditions the energy channeled through the KrF* molecule represents between 20 and 30 percent of the total discharge energy (Fig.1 9). Note, however, that both the contributions of positive

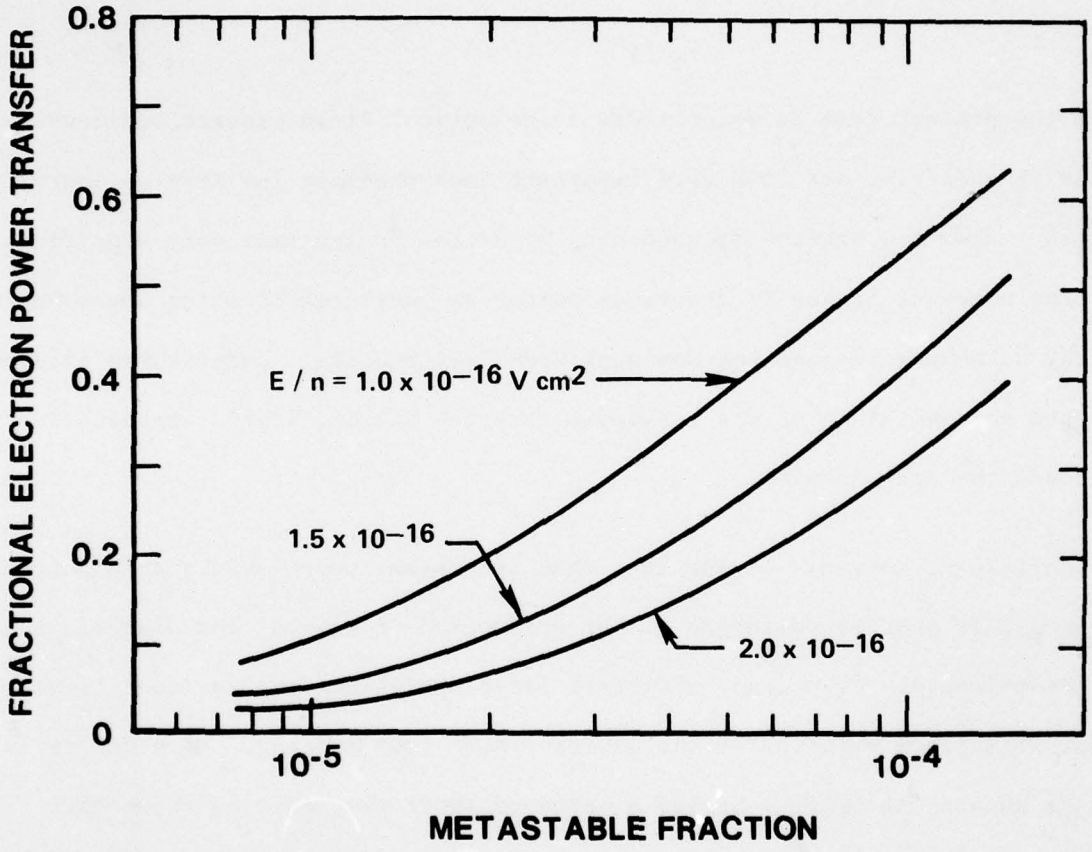

Fig. 14 Fractional loss of electron power resulting from the net effect of excitation and de-excitation of the rare gas p states in an Ar-Kr-F_2 (0.945-0.05-0.005) mixture. The fraction of p state atoms was maintained at a value one-tenth that of the metastable fraction for the purposes of this illustration.

78-06-7-18

ion-negative ion recombination and of the direct reaction of F_2 with krypton metastables are also significant. The relative importance of the Kr*-F_2 reaction will be even larger for values of Kr fractional concentration larger than the 0.05 considered here.

For the present case in which there is no optical field present, spontaneous decay and F_2 quenching are both very important loss channels for KrF* as indicated in Fig. 16. However, three-body quenching by Ar and Kr are also very significant. Indeed, for somewhat higher Kr fractions and/or at pressures of a few atmospheres three-body quenching becomes the dominant KrF* loss process. Under these circumstances the concentration of the triatomic rare-gas halide, Kr_2F^*, approaches and even exceeds the KrF* density.

Of particular interest is the fact that in e-beam controlled, discharge pumped lasers no single process dominates either production or loss of the diatomic rare-gas halide molecule. Of course, efficient laser operation requires conditions such that stimulated emission is the dominant KrF* loss process. With the ratio of gain to absorption (g_o/γ_o) having a value of about ten, analysis shows that efficient optical power extraction requires an optical flux approximately twice the saturation level[1], the latter having a value of nearly 1 MW cm^{-2} for the conditions of Fig. 16.

C. F_2 Dissociation

The results and discussion presented above show that optimum conditions for efficient production of KrF* can be achieved in high-power e-beam controlled (or e-beam excited) lasers. In addition it is shown that F_2 exerts a very important

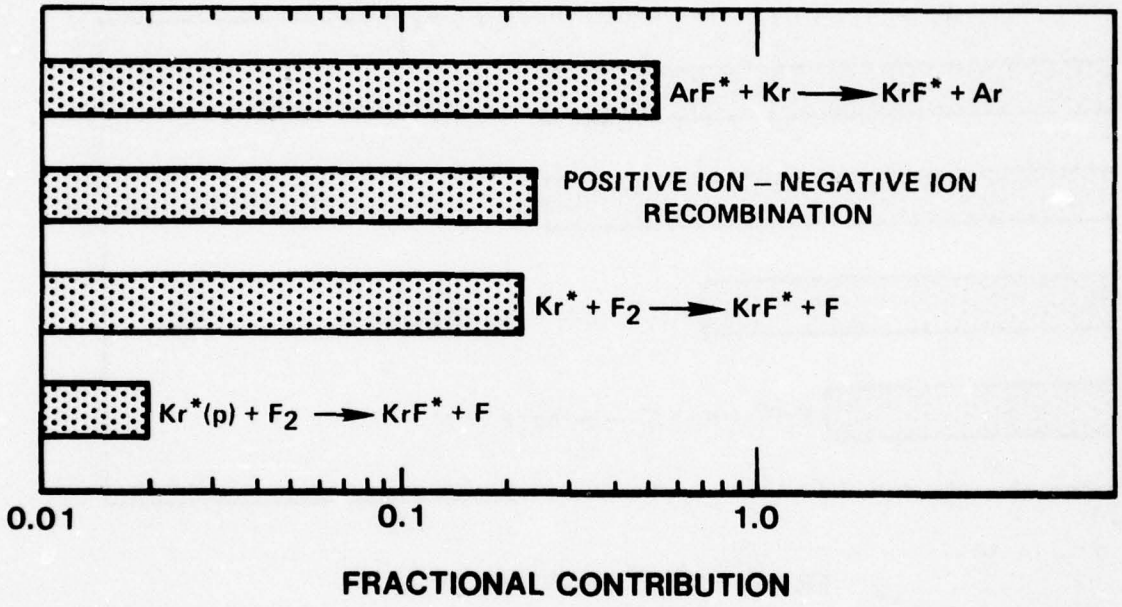

Fig. 15 Fractional contributions to KrF* production in an e-beam controlled laser discharge for the conditions of Fig. 7.

78-06-7-9

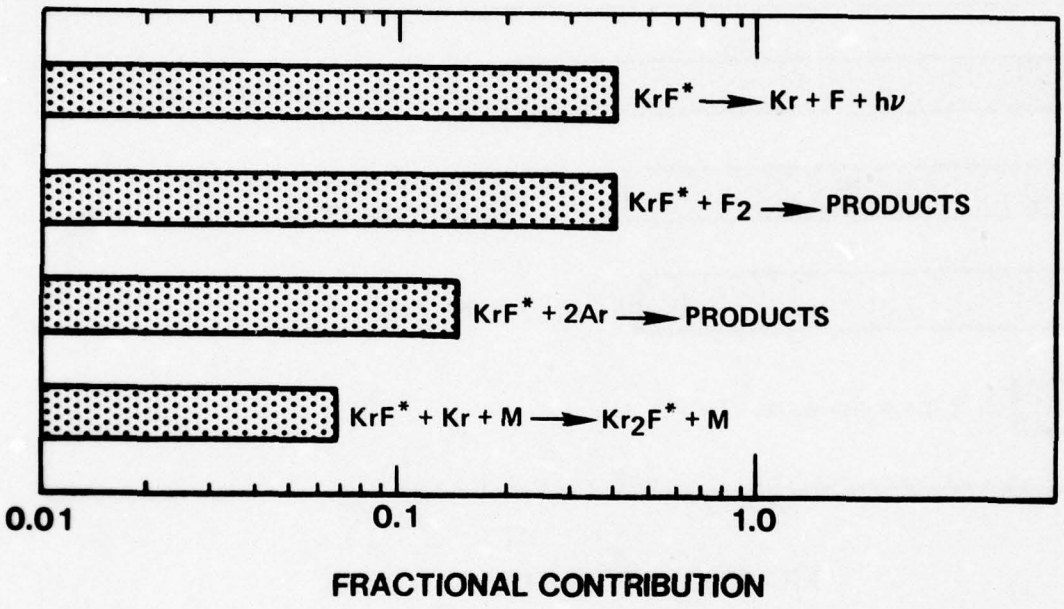

Fig. 16 Fractional contributions to KrF* loss (in the absence of a radiation field) for the conditions of Fig. 7.

78-06-7-14

(indeed dominant) influence on the concentrations of electrons, metastable and p-state atoms, and rare-gas halide molecules. Thus, no single process exerts an influence on laser plasma conditions which is comparable to the effects of F_2 dissociation. Figure 7 shows that substantial F_2 dissociation can occur in a time less than 1 μsec in e-beam controlled discharges. Although plasma conditions are quite satisfactory for the first 0.5 μsec for this example (Fig. 9), as a result of dissociation a substantial variation in properties occurs for times in excess of about 0.6 μsec, resulting in the occurrence of plasma instability shortly thereafter.

The various contributions to F_2 dissociation for these conditions are presented in Fig. 17. By far the most important feature of this figure is its indication of the large number of different processes resulting in dissociation. Clearly, F_2 dissociative reactions are of a fundamental nature in rare-gas halide lasers. Indeed, because of the large number of reactions involved, numerical experimentation shows that the quasi-steady plasma properties discussed in previous paragraphs are relatively insensitive to variations in the rate coefficients used for the reactions indicated in Fig. 17, within known limits of uncertainty. However, since ionization resulting form low energy electron impact is always important (Fig. 11) for the conditions of primary interest, the plasma is only marginally stable. For this reason the time at which instability actually occurs can vary significantly in response to changes in the F_2 concentration.

D. Plasma Instability

For the electrical power density values required for optimum laser performance the loss of F_2 due to dissociation, along with gas heating, establishes a

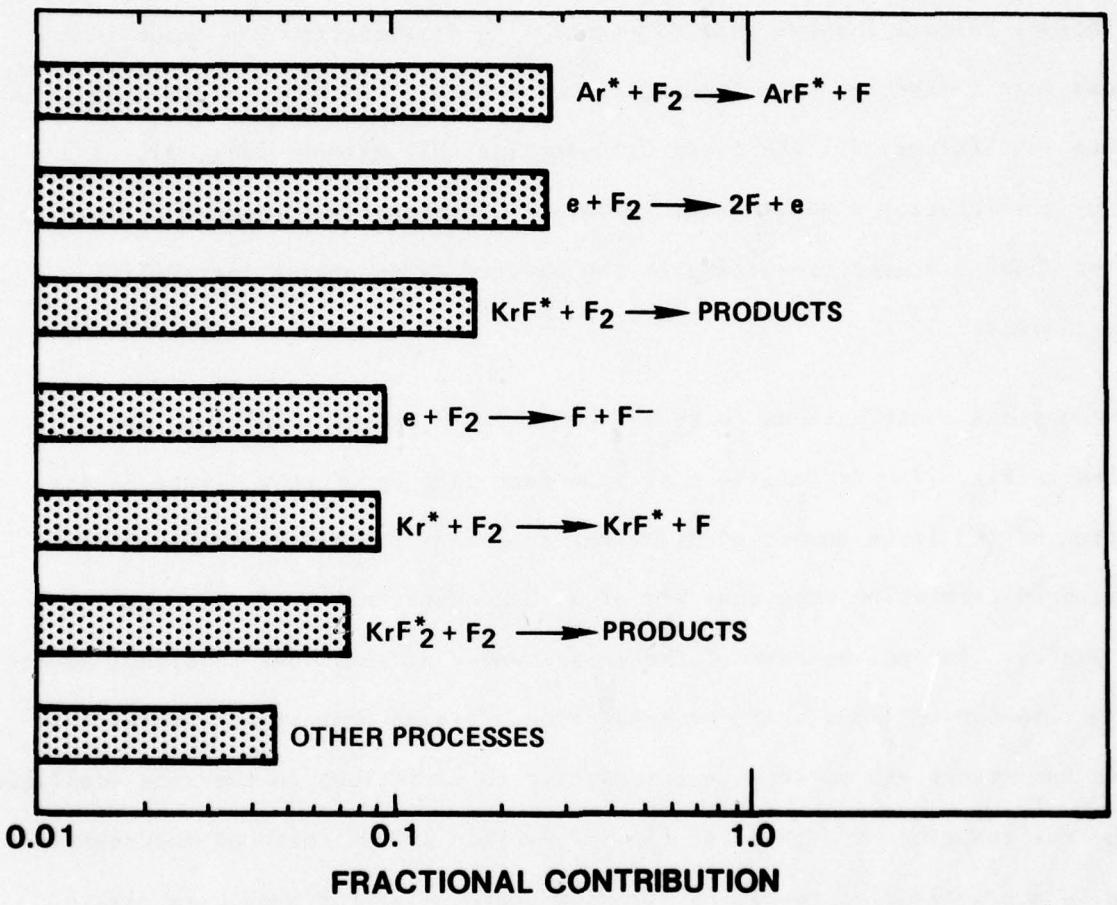

Fig. 17 Fractional contributions to F_2 dissociation in an e-beam controlled KrF* laser discharge for the conditions of Fig. 7.

78-06-7-13

maximum limit for discharge pulse length which is on the order of a few μsec. However, the occurrence of plasma instability (current runaway) in a much shorter time actually determines the maximum attainable pulse duration in e-beam controlled rare-gas halide lasers.[1,31,33,34,35] For this reason plasma instability plays a uniquely important role in determining the experimentally accessible range of laser discharge operating parameters, especially discharge : e-beam power enhancement factor,[1] (Fig. 9).

Electron Density Growth

Completely self-consistent analysis of rare-gas halide laser stability is a formidable problem, requiring consideration of the temporal response of the electrons, ions and several excited species to disturbances in plasma properties. However, the mode of instability leading to current runaway in rare-gas halide discharges has been identified as ionization instability.[1,31,36,37] This instability is a manifestation of temporal amplification of electron density disturbances. Therefore, useful insight can be obtained by consideration of the time dependent electron conservation equation alone. For the present purpose this equation may be expressed in the form,

$$\frac{\partial n_e}{\partial t} \simeq nS + n_e n k_i + n_e n^* k_i^* + n_e n^*(p) k_i^*(p) - n_e n_{F_2} k_a , \qquad (1)$$

where n_e, n, n^*, $n^*(p)$ and n_{F_2} are the densities of electrons, ground state neutrals, metastables, p-state atoms and F_2, respectively, S is ionization rate due to the external source, and k_i, k_i^* and $k_i^*(p)$ are the rate coefficients for ionization of ground state atoms, metastable atoms and p-state atoms (Figs. 3-6), and k_a is the F_2 attachment rate coefficient. If it is assumed that excited species respond to disturbances on at time scale which is shorter than

that of the electrons[a], and that electron density disturbances vary as exp(υ), application of first order perturbation theory results in the following approximate expression for the maximum growth rate of electron density disturbances:

$$\nu \simeq nk_i \left(1 + \frac{\alpha}{k_i}\frac{\partial k_i}{\partial \alpha}\right) + 2n^* k_i^* + 3n^*(p)\, k_i^*(p) - n_{F_2} k_a \qquad (2)$$

The first term on the right hand side is the contribution of ground state ionization; thus the term $(\alpha/k_i)\partial k_i/\partial\alpha$ is a dimensionless quantity of order unity which reflects the variation in the ionization rate coefficient with changes in fractional ionization, α, (Fig. 4). The second and third terms reflect the influence of metastable and p-state ionization, respectively, the factor-of-two arising because the metastable concentration varies as the square of the electron density, and the factor-of-three because the density of p-state atoms varies as the cube of the electron density. In order to ensure stability ($\upsilon < 0$, electron density disturbances damped), the attachment term $n_{F_2}k_a$, must always be larger than the combined contributions to Eq. (2) from the various ionization processes.

Presented in Fig. 18 are the temporal variations of the dominant contributions to Eq. (2) for the conditions of Fig. 7, i.e., excited state ionization and attachment to F_2 (in the ground vibrational state). Initially, conditions are such that the contribution due to ionization from excited states is safely below that

---

(a) Although electrons and metastable atoms often respond to disturbances on the same time scale, the approximation that perturbations in the metastable concentration are quasi-steady significantly simplifies analysis, thereby facilitating development of insight as regards the causes of ionization instability.

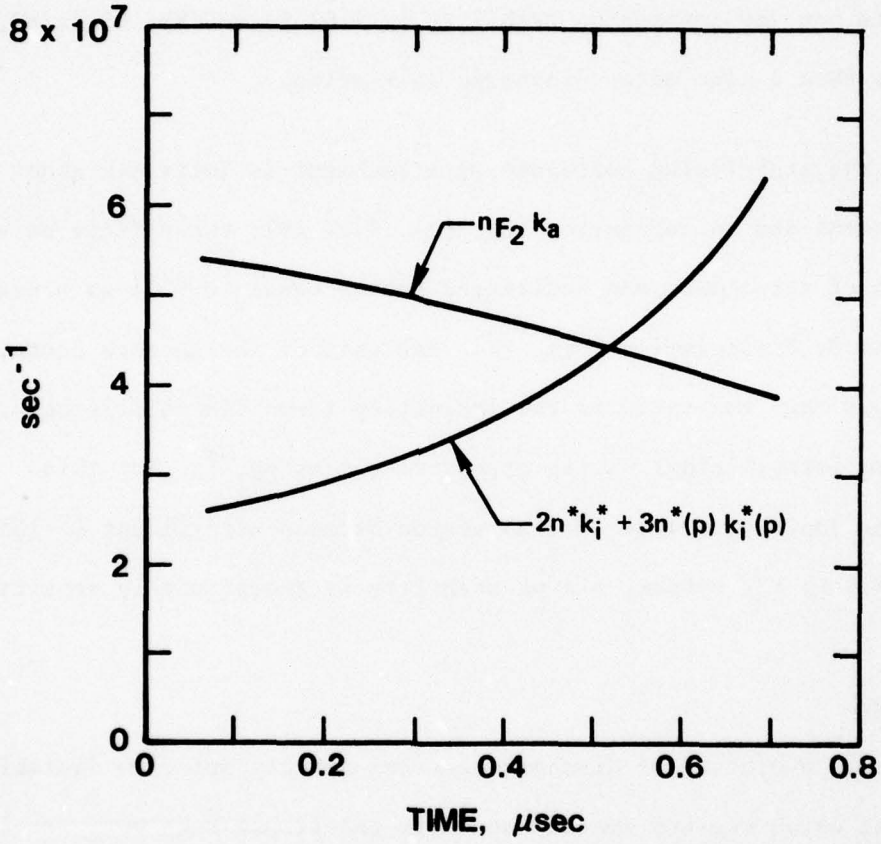

Fig. 18 First order contributions to the growth (or damping) rate of electron density disturbances resulting from ionizaton of Ar and Kr excited states and from dissociative attachment to F_2 in the ground vibrational state for the conditions of Fig. 7.

78-06-7-5

due to attachment, the latter effectively balanced by ionization provided by the external source (Fig. 11). However, as the F_2 concentration decreases as a result of dissociation, this situation changes significantly with ionization from excited states increasing by about a factor of two in only a few tenths of a μsec. Thus, the criterion for ionization stability ($\upsilon < 0$) is quickly violated, usually in a time less than 1 μsec after discharge initiation.

Although the stabilizing influence of attachment is initially about twice as large as the terms due to ionization (Eq. (2), Fig. 18), the effects on electron density growth of attachment and ionization become equal ($\upsilon = 0$) as a result of only 25 percent F_2 dissociation (Fig. 7). Analysis of the factors contributing to Eq. (2) shows that the ratio of the ionization terms (destabilizing) to the attachment term (stabilizing) varies approximately as $n_{F_2}^{-3}$. For this reason whenever ionization from excited states becomes significant (> 10%) relative to that provided by the e-beam, plasma stability is exceptionally sensitive to the loss of F_2.

Current Runaway

The temporal evolution of discharge current density prior to instability onset and the time at which current runaway actually occurs are both very sensitive to the discharge E/n value. Figure 19 presents computed current density profiles for various E/n values and conditions otherwise similar to those discussed previously. The discharge : e-beam power enhancement factor at the leading edge of the pulse is also indicated. Although the current density is uniform and the plasma is stable for over 1 μsec at an E/n value of 1.0×10^{-16} Vcm^2, at this value the power

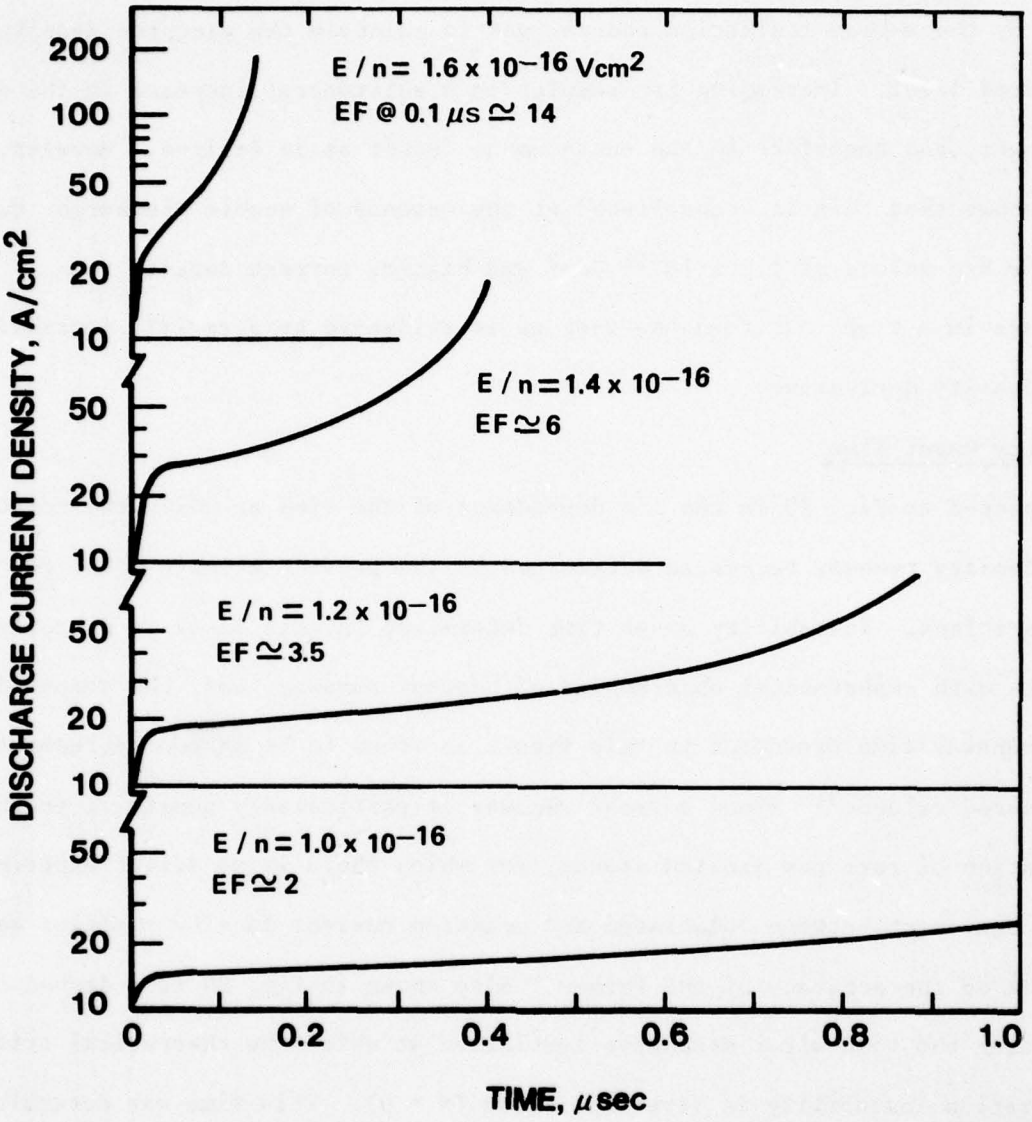

Fig. 19 Temporal variation of discharge current density for various E/n values and conditions otherwise the same as Fig. 7. The indicated values of discharge: e-beam power enhancement factor refer to the time 0.1 μsec after discharge initiation.

78-06-7-4

enhancement factor is only about two. That is, about 1/3 of the total power is provided by the e-beam ionization source just to maintain the electron density at the required level. Increasing E/n results in a substantial increase in the discharge power, and therefore in the enhancement factor as is desired. However, Fig. 19 shows that this is accomplished at the expense of stable discharge duration. For E/n values of 1.2×10^{-16} Vcm^2 and higher, current density runaway occurs in a time less than one μsec as is evidenced by a rapidly increasing current density derivative.

Instability Onset Time

Presented in Fig. 20 is the E/n dependence of the time at which the computed current density runaway occurs as determined by the present kinetic model for KrF* laser conditions. Instability onset time determined on this basis is directly comparable with experimental observation of current runaway; and, the computed current runaway time presented in this figure is found to be in good agreement with measured values.[31] Since current runaway is particularly sensitive to the concentration of rare gas excited states, for which there is no direct experimental measure, agreement between calculated and measured current density profiles serves as a check on the accuracy of the former. Also shown in Fig. 20 is a dashed curve representing the time after discharge initiation at which the theoretical criterion for ionization instability is first satisfied ($\upsilon = 0$). This time was determined by computing the instability growth (or damping) rate using time varying plasma conditions to evaluate Eq. 2. For low values of E/n the plasma is stable for a relatively long time ($\sim$ 1 μsec). Under these conditons the computed instability onset time based on the theoretical criterion ($\upsilon = 0$) and on the current runaway time as determined from the complete kinetics calculation are essentially equivalent,

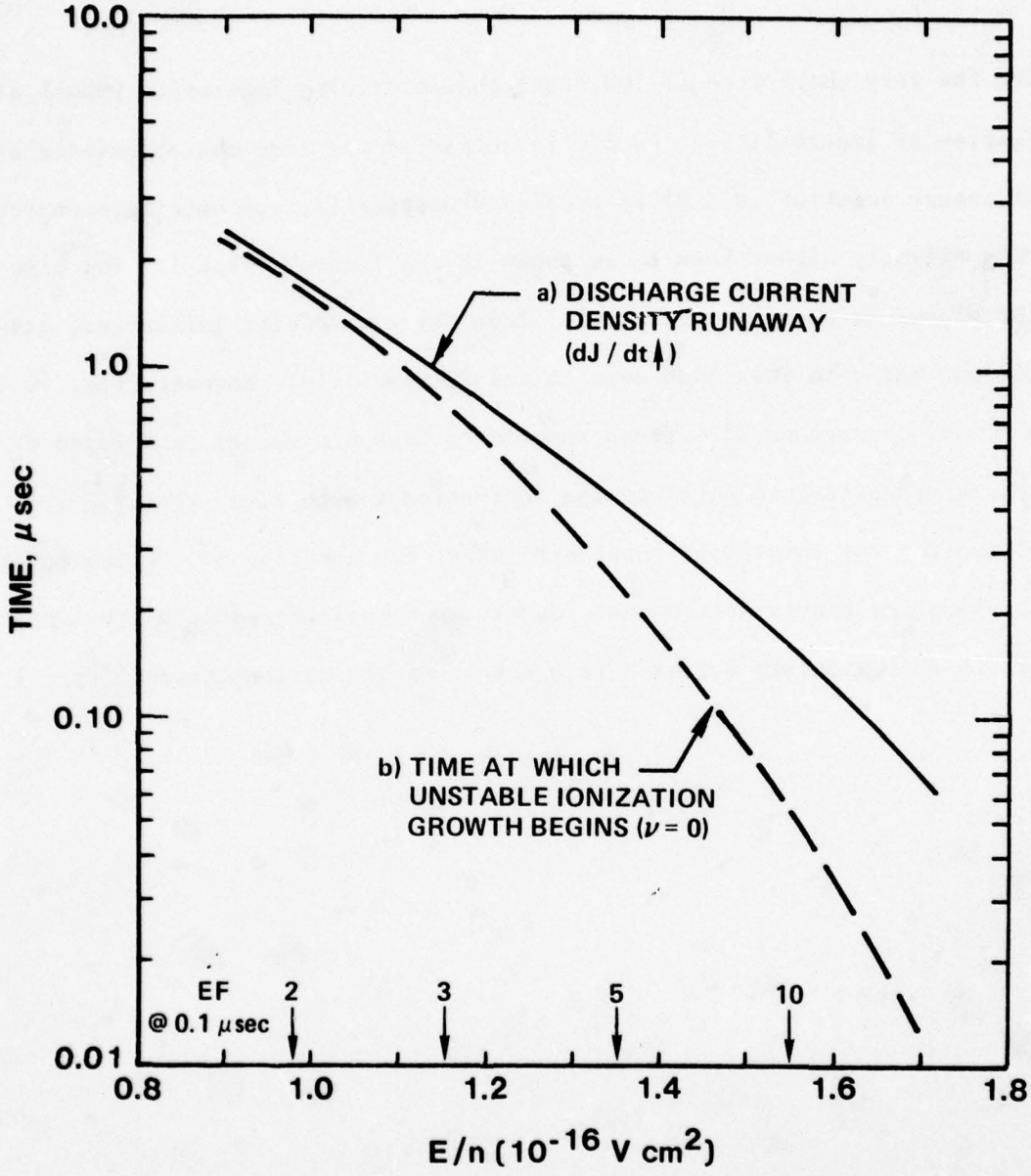

Fig. 20 E/n variation of the time after discharge initiation at which numerically determined current runaway begins (curve a); and at which exponential growth of electron density disturbances begins, i.e. ionization instability (curve b). In the evaluation of curve b (υ=0) ionization of ground state atoms and attachment of vibrationally excited F_2 were taken into account. These results correspond to the conditions of Fig. 7.

78-06-7-16

reflecting the very short time (< 100 nsec) characterizing ionization growth after the initiation of instability.[a] As E/n is increased the time characteristic of stable discharge duration ($\upsilon < 0$) is reduced dramatically, approaching zero for E/n values only slightly higher than those shown in the figure. That is, for high E/n values the plasma is unstable practically from the time of its initiation, based on the criterion that υ be less than zero to ensure stability. However, Fig. 20 shows that the actual occurrence of current runaway at high E/n values is delayed by a time which is approximately equal to the ionization growth time, $\sim(n^*k_i)^{-1}$. Nevertheless, for the conditions considered here, the duration of the excitation pulse for which the energy enhancement factor can be maintained at a level near ten is limited to approximately 0.1 μsec as a result of ionization instability.

(a) On the basis of this comparison it can also be concluded that the factors dominating ionization instability in rare-gas halide lasers are reasonably represented by the approximate expression for the instability growth rate given in Eq. (2).

IV. SUMMARY AND DISCUSSION

The analysis and discussion of the preceding sections focuses attention on the relationship among the numerous processes contributing to the formation and loss of the KrF* molecule in an electron-beam controlled discharge. Therein it is shown that KrF* can be produced with an efficiency of 20 percent using this scalable excitation technique. In addition, krypton-monofluoride densities in excess of 10^{14} cm^{-3} are readily attained which, when combined with a stimulated emission cross-section of about 2.4×10^{-16} cm^2, results in a gain coefficient of about 1 percent cm^{-1}. Thus, it can be concluded that KrF* kinetic processes are generally very favorable for efficient laser operation under conditions typical of near atmospheric pressure electron-beam controlled discharges.

The plasma required to achieve optimum KrF* laser excitation is characterized by a mean electron energy of several electron-volts, a fractional ionization greater than 10^{-6}, and a fractional metastable concentration in excess of 10^{-5}. Section II shows that under these conditions electron-electron collisions and electron collisions with excited atoms have a very important effect on plasma processes. Further, it is shown that numerous reactions, including rare-gas halide formation, result in dissociation of the fluorine fuel molecules. Since reactions between halogen molecules and both metastable atoms and electrons exert a controlling influence on the population of these species, dissociation of F_2 results in significant changes in plasma properties. Indeed, the results presented here show that as a result of F_2 dissociation, KrF* laser properties are continuously changing from the time of plasma initiation until termination due either to the onset of instability or to critical loss of F_2. For values of discharge :

e-beam power enhancement greater than about three, results obtained to date have shown that plasma instability limits maximum laser pulse duration to a time less than 1 μsec (Figs. 19-20). However, with E/n values corresponding to enhancement factors in the 2-3 range, laser pulses of about 1 μsec have been achieved[1], with eventual loss of F_2 being the factor limiting pulse duration. This general behavior is typical of all electron-beam controlled rare-gas halide lasers[1,35] and of the closely related mercury-halide[38] lasers as well.

Based on the good agreement between measured and predicted laser characteristics, it is reasonable to conclude that the dominant reactions influencing rare-gas halide formation and loss have been identified and that a satisfactory data base exists. However, operational experience with rare-gas halide lasers has, for the most part, been limited to single pulse experiments.[1] Practical implementation of this unusually promising class of high-power lasers requires dependable, repetitive pulse operation using a flowing, recirculating gas mixture. In addition, many applications will require electron-beam controlled discharge excitation under conditions such that the e-beam power is a relatively small fraction (< 0.1) of the discharge power. Past experience with ir molecular lasers indicates that the major obstacles to achieving these objectives will be related to plasma chemical processes and discharge stability.[39-41] Solution of these formidable problems will require substantial additions to the existing body of knowledge pertaining to rare-gas halide kinetics. Aside from the primary reactions directly involved in rare-gas halide molecular processes, very little data exists for reactions between halogen molecules (and atoms) and discharge species. For example, there is little or no information pertaining to the reaction of either F

atoms or F_2 with rare-gas excited states, electrons or ions.[42] While reactions of this type may play only a secondary role in rare-gas monohalide molecule formation and loss as it occurs in a single pulse experiment, they are certain to exert an important influence on the chemistry of closed-cycle, repetitive pulse lasers.

Analysis of positive ion reactions in rare-gas halide plasmas is based almost entirely on the premise that rare-gas monomer and dimer ions are dominant. However, in addition to these ions, rare-gas trimer ions, heteronuclear rare-gas dimer ions and rare-gas halide ions are likely to be present in significant concentrations ($\sim$ 10 percent). It is known that relatively small concentrations of complex ions can significantly influence plasma properties[43] (especially stability[41]) because of their unusually large electron recombination coefficients.[44] In addition, positive ions play a unique role in rare-gas halide lasers as a consequence of their direct involvement in rare-gas halide formation[1,5] and because they absorb radiation at the laser wavelength.[32,45] For these reasons, improved knowledge of ion reactions at high pressure and low temperature is also of importance, especially under closed-cycle conditions for which the concentration of neutral species produced by plasma-chemical reactions is likely to become substantial.

Experimental verification[1] of the high energy conversion efficiency predicted for the KrF* laser represents a significant milestone in the development of a scalable, high power uv laser, and provides impressive evidence that conditions optimum for efficient laser excitation can be created in a high pressure, chemically active plasma. However, it has also been found that it is exceptionally difficult to maintain the desired plasma properties in a stable, long pulse ($\sim$ μsec) discharge

because of significant changes in the gas mixture arising from the rare-gas halide formation process itself. As these systems are scaled for applications requiring high average power, difficulties arising from this circumstance will certainly become more pronounced. For this reason it is clear that future efforts must be directed toward identification of the dominant ion and neutral chemical reactions occurring under the plasma conditions to be encountered with closed-cycle, respectively pulsed rare-gas halide lasers.

ACKNOWLEDGEMENTS

It is a pleasure to acknowledge the comments of R. T. Brown, which were particularly helpful in the preparation of this paper. Useful discussions with R. H. Bullis, H. H. Michels, L. A. Newman and and W. J. Wiegand are also appreciated.

REFERENCES

* Portions of this work were supported by the Office of Naval Research.

1. M. Rokni, J. A. Mangano, J. H. Jacob and J. C. Hsia, "Rare gas-fluoride lasers," IEEE J. Quantum Electron, (in press); and references cited herein.
2. J. J. Ewing, "Rare-gas halide lasers," Physics Today, vol. 31, pp. 32-39, May 1978.
3. J. E. Velazco and D. W. Setser, "Bound-free emission spectra of diatomic xenon halides," J. Chem. Phys. vol. 62, pp. 1990-1991, 1 March 1975.
4. P. J. Hay and T. H. Dunning Jr., "The electronic states of KrF," J. Chem. Phys., vol. 66, pp. 1306-1316, February 1977.
5. M. Rokni, J. H. Jacob, and J. A. Mangano, "Dominant formation and quenching processes in e-beam pumped ArF* and KrF* lasers," Phys. Rev. A, vol. 16, pp. 2216-2224, December 1977.
6. J. H. Jacob and J. A. Mangano, "Modeling the KrF* laser discharge," Appl. Phys. Lett., vol. 28, pp. 724-726, 15 June 1976.
7. W. B. Lacina and D. B. Cohn, "Theoretical analysis of the electrically excited KrF* laser," Appl. Phys. Lett., vol. 32, pp. 106-108, 15 January 1978.
8. A. J. DeMaria, "Review of High-Power CO_2 Lasers," Principles of Laser Plasmas, (G. Bekefi, Ed.), New York: John Wiley and Sons, 1976.
9. J. D. Daugherty, "Electron-beam ionized lasers," Principles of Laser Plasmas, (G. Bekefi, Ed.), New York : John Wiley and Sons, 1976.
10. W. L. Nighan, "Influence of molecular dissociation and degree of ionization on rare-gas halide laser properties," Appl. Phys. Lett., vol. 32, pp. 424-426, 1 April 1978.
11. R. J. Hall, "Dissociative attachment and vibrational excitation of F_2 by slow electrons," J. Chem. Phys., vol. 68, pp. 1803-1807, 15 February 1978.

12. W. L. Nighan, "Influence of electron-F_2 collisions in rare-gas halide laser discharges," Appl. Phys. Lett., vol. 32, pp. 297-300, 1 March 1978.

13. P. J. Hay and D. C. Cartwright, "Rydberg, ionic and valence interactions in the excited states of F_2," Chem. Phys. Lett., vol. 41, pp. 80-82, 1 July 1976.

14. M. V. Kurepa and D. S. Belic, "Dissociative attachment of electrons to chlorine molecules," Chem. Phys. Lett., vol. 49, pp. 608-610, 1 August 1977.

15. W. C. Tam and S. F. Wong, "Dissociative attachment of halogen molecules by 0-8 eV electrons," J. Chem. Phys. (to be published).

16. P. J. Chantry, "Attachment measurements in halogen bearing molecules," (to be published).

17. W. L. Borst, "Excitation of metastable argon and helium atoms by electron impact," Phys. Rev. A, vol. 9, pp. 1195-1200, March 1974.

18. D. Rapp and P. Englander-Golden, "Total cross sections for ionization and attachment in gases by electron impact. I. Positive ionization," J. Chem. Phys., vol. 43, pp. 1464-1479, 1 September 1963.

19. S. D. Rockwood, "Elastic and inelastic cross-sections forelectron-Hg scattering from Hg transport data," Phys. Rev. A., vol. 8, pp. 2348-2358, November 1973.

20. W. H. Long, Jr., "Electron kinetics in the KrF laser," Appl. Phys. Lett., vol. 31, pp. 391-393, 15 September 1977.

21. H. A. Hyman, "Electron impact excitation of metastable argon and krypton," Phys. Rev. A (to be published).

22. D. Ton-That and M. R. Flannery, "Cross sections for ionization of metastable rare-gas atoms (Ne*, Ar*, Kr*, Xe*) and of metastable N_2*, CO* molecules by electron impact," Phys. Rev. A , pp. 517-526, February 1977.

23. Cross sections for ionization of rare gas atoms from their p states were obtained using Gryzinski's formula (Phys. Rev., vol. 138, pp. A336-A358, 19 April 1963). As a check on the validity of this approximation for the conditions of interest, Gryzinski cross sections for ionization of rare gas metastable states were generated and were found to be in good agreement with those of Ref. 22.

24. W. L. Nighan, "Electron energy distributions and collision rates in electrically excited N_2, CO, and CO_2," Phys. Rev. A , vol. 2, pp. 1989-2000, November 1970.

25. J. E. Velazco, J. H. Kolts and D. W. Setser, "Quenching rate constants for metastable argon, krypton, and xenon atoms by fluorine containing molecules and branching ratios for XeF* and KrF* formation," J. Chem. Phys., vol. 65, pp. 3468-3480, 1 November 1976.

26. L. G. Piper and D. W. Setser, "Electronic energy transfer from metastable argon atoms to krypton atoms.", J. Chem. Phys., vol. 63, pp. 5018-5028, 1 December 1975.

27. G. P. Quigley and W. M. Hughes, "The radiative lifetime and quenching of KrF," Appl. Phys. Lett., vol. 32, pp. 627-629, 15 May 1978; also, J. G. Eden, R. W. Waynant, S. K. Searles and R. Burnham, "New quenching rates applicable to the KrF lasers," Appl. Phys. Lett., vol. 32, pp. 733-735, 1 June 1978.

28. G. P. Quigley and W. M. Hughes, "Lifetime and quenching rate constants for Kr_2F* and Kr*, "Appl. Phys. Lett., vol. 32, pp. 649-651, 15 May 1978.

29. P. J. Hay and T. H. Dunning, "The covalent and ionic states of the rare-gas monofluorides," J. Chem. Phys. (to be published).

30. R. S. F. Chang and D. W. Setser, "Radiative lifetimes and two-body deactivation rate constants for $Ar(3p^5,4p)$ and $Ar(3p^5,4p')$ states," J. Chem. Phys. (to be published).

31. R. T. Brown and W. L. Nighan, "Instability onset in electron-beam sustained KrF* laser discharges," Appl. Phys. Lett., vol. 32, pp. 730-732, 1 June 1978.

32. A. M. Hawryluk, J. A. Mangano and J. H. Jacob, "Gain and absorption measurements in a KrF* laser," Appl. Phys. Lett., vol. 31, pp. 164-166, 1 August 1977.

33. C. H. Fisher and R. E. Center, "Threshold power density measurements for electron-beam sustained discharge excitation of XeF* and KrF*, Appl. Phys. Lett., vol. 31, pp. 106-108, 15 July 1977.

34. J. A. Mangano, J. H. Jacob and J. B. Dodge, "Electron-beam controlled discharge pumping of the XeF laser," Appl. Phys. Lett., vol. 29, pp. 426-428, 1 October 1976.

35. L. F. Champagne and N. W. Harris, "Characteristics of the electron-beam controlled XeF laser," Appl. Phys. Lett. (to be published).

36. J. D. Daugherty, J. A. Mangano and J. H. Jacob," Attachment dominated electron-beam ionized discharges," Appl. Phys. Lett., vol. 28, pp. 581-583, 15 May 1976.

37. W. H. Long, Jr., "Discharge stability in e-beam sustained rare-gas halide lasers," (to be published).

38. J. H. Parks, "Laser action on the $B^2\Sigma^+_{1/2} \rightarrow X^2\Sigma^+_{1/2}$ band of HgCl at 5576 A^o, Appl. Phys. Lett., vol. 31, pp. 192-194, 1 August 1977; also, W. T. Whitney, "Sustained discharge excitation of HgCl and HgBr $B^2\Sigma^+_{1/2} \rightarrow X^2\Sigma^+_{1/2}$ lasers," Appl. Phys. Lett., vol. 32, pp. 239-241, 15 February 1978.

39. W. L. Nighan, "Stability of high-power molecular laser discharges," Principles of Laser Plasmas (G. Bekefi, Ed.), New York: John Wiley and Sons, 1976.

40. W. L. Nighan, "Causes of thermal instability in externally sustained molecular discharges," Phys. Rev. A , vol. 15, pp. 1701-1720, April 1970.

41. W. L. Nighan, "Influence of recombination and ion chemistry on the stability of externally sustained molecular discharges," Phys. Rev. A , vol. 16, pp. 1209-1223, September 1977.

42. E. W. McDaniel, M. R. Flannery, H. W. Ellis, F. L. Eisele, W. Pope and T. G. Roberts, "Compilation of data relevant to rare gas-rare gas and rare gas-monohalide excimer lasers: volumes 1 and 2," Rept. H-78-1, U. S. Army Missile Research and Development Command (DRDMI-TI), December 1977.

43. C. W. Werner, E. Zamir and E. V. George, "Pressure dependence of the electron density in electron-beam-excited rare-gas plasmas," Appl. Phys. Lett., vol. 29, pp. 236-239, 15 August 1976.

44. M. A. Biondi, "Recombination," Principles of Laser Plasmas (G. Bekefi, Ed.), New York: John Wiley and Sons, 1976.

45. W. R. Wadt, D. C. Cartwright and J. S. Cohen, "Theoretical absorption spectra for Ne_2^+, Ar_2^+, Kr_2^+, and Xe_2^+ in the rear ultraviolet," Appl. Phys. Lett., vol. 31, pp. 672-674, 15 November 1977.

APPENDIX

REPRINTS OF PUBLISHED PAPERS

W. L. Nighan, "Influence of electron-F_2 Collisions in rare gas-halide laser discharges", Applied Physics Letters, Vol. 32, pp. 297-300, 1 March 1978.

W. L. Nighan, "Influence of molecular dissociation and degree of ionization on rare gas-halide laser properties", Applied Physics Letters, Vol. 32, pp. 424-426, 1 April 1978.

R. T. Brown and W. L. Nighan, "Instability onset in electron-beam-sustained KrF* laser discharges", Applied Physics Letters, Vol. 32, pp. 730-732, 1 June 1978.

R. J. Hall, "Dissociative attachment and vibrational excitation of F_2 by slow electrons", Journal of Chemical Physics, Vol. 68, pp. 1803-1807, 15 February 1978.

Influence of electron-F_2 collisions in rare gas–halide laser discharges[a)]

William L. Nighan

United Technologies Research Center, East Hartford, Connecticut 06108
(Received 23 September 1977; accepted for publication 20 December 1977)

The influence of F_2 vibrational excitation and direct dissociation by electron impact is examined for conditions typical of electron-beam-sustained KrF* lasers. For values of F_2 fractional concentration greater than about 0.003 the results of this analysis indicate that the dissociation process $e + F_2 \rightarrow 2F + e$ may significantly affect electron-metastable atom production efficiency, rare gas–halide excimer production efficiency, and gain.

PACS numbers: 42.55.Hq, 52.20.Fs, 52.20.Hv

Rare gas–halide laser mixtures generally contain fractional concentrations of the halogen bearing molecule in the 0.1–1.0% range. Although there exists almost no electron scattering data for such molecules, there is every reason to suppose that the presence of several tenths of a percent F_2, for example, will have an effect on electron kinetics other than by way of the well-known dissociative attachment process. This paper analyzes available data relevant to electron-F_2 scattering and examines the potential importance of such collision processes for conditions typical of discharge-pumped KrF* lasers.

To date the effect of electron-halogen molecule inelastic collisions has not been considered in analyses of rare gas–halide lasers. This is a reflection of the lack of required cross-section data. However, recent theoretical analysis[1] has shown that vibrational excitation of F_2 by electrons can proceed by way of a resonance mechanism involving the same F_2^- state which participates in the low-energy dissociative attachment process. The computed energy weighted cross section for vibrational excitation was found to be in excess of 10^{-17} cm^2 in the electron energy range of a few electron volts. In addition, measurements[2] of F atom production in an electron-beam-sustained F_2 discharge have shown evidence of enhanced F_2 dissociation as E/n was increased for average electron energies estimated to be about 1 eV, a value high enough[1] so that dissociative attachment should be a decreasing function of E/n. While there are several processes[2] which may contribute to F_2 dissociation for the experimental conditions of Ref. 2, direct electron impact dissociation is by far the most likely. Indeed, there are several F_2^- states which may lie above the repulsive $F_2(^1\pi_u)$ state in the vicinity of the F_2 ground-state equilibrium separation, so that resonant enhancement of the process $e + F_2 \rightarrow 2F + e$ is a distinct possibility.

a)Portions of this work were supported by the Office of Naval Research.

 0003-6951/78/3205-0297$00.50

In order to obtain an estimate for the electron-F_2 dissociation cross section based on the observations of Ref. 2, electron energy distributions were computed for F_2 using the vibrational cross sections of Ref. 1 along with a constant momentum transfer cross section having a value of 10^{-15} cm^2. The electron-F_2 dissociation cross section was assumed to have an apparent threshold of 3.35 eV corresponding to the vertical transition energy from the F_2 ground state to the $F_2(^1\pi_u)$ state, the lowest electronic state of F_2. The magnitude and shape of this cross section were then varied in a trial and error fashion. In the experiments of Ref. 2 the production of F atoms was first observed to increase over that due to the electron beam alone for an E/n value of approximately 2×10^{-16} V cm^2. As E/n was increased to about 6×10^{-16} V cm^2, F atom production was enhanced by almost a factor of 2. By using a trial dissociation cross section having a peak value of approximately 10^{-17} cm^2 at an electron energy of 5 eV, in the present work it was found that the magnitude of the calculated rate of F_2 dissociation (F atom production) by the direct process was a few percent of that due to dissociative attachment for an E/n of 2×10^{-16} V cm^2. Further, the dissociation rate approximately equaled the dissociative attachment rate for E/n values in the 5×10^{-16} to 6×10^{-16}-V cm^2 range, results consistent with the experimental observations.[2] These findings were not particularly sensitive to the shape of the trial cross section used in the analysis. The direct electron-F_2 dissociation rate estimated in this manner is consistent with the limited experimental data available[2] and provides a reasonable basis for an evaluation (albeit provisional) of the potential significance of electron impact excitation of F_2 to repulsive states.

Using this F_2 dissociation cross section and the cross sections of Ref. 1 the electron fractional power transfer

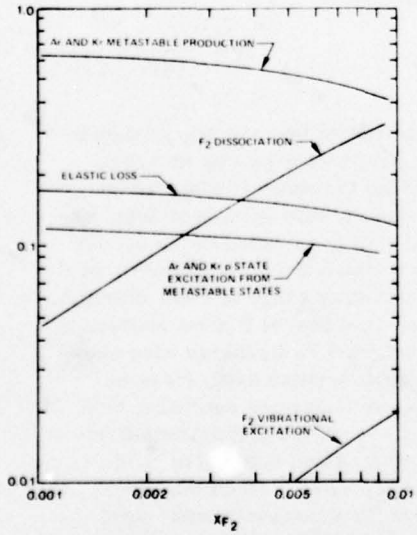

FIG. 1. Contributions to electron fractional power transfer in an Ar-Kr-F_2 mixture in which the Ar and Kr fractional concentrations were 0.95 and 0.05, respectively. The calculation was carried out for an E/n value 1.0×10^{-16} V cm^2, a fractional metastable concentration of 10^{-5}, and a fractional ionization of 10^{-6}.

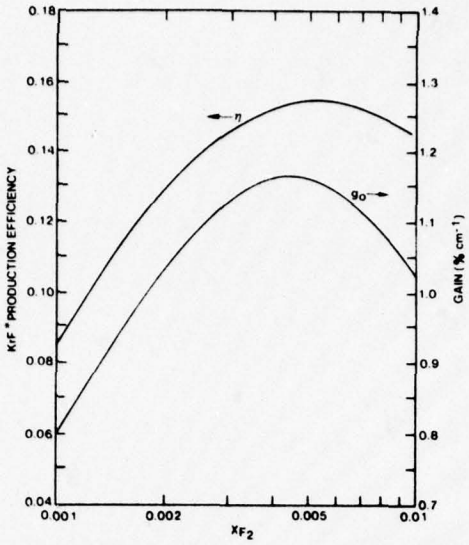

FIG. 2. Small-signal gain and KrF* production efficiency in an electron-beam-sustained discharge as a function of F_2 fraction. The computation was made for an atmospheric-pressure Ar-Kr (0.95—0.05) mixture and an E/n value of 1.0×10^{-16} V cm^2. These results refer to conditions 100 nsec after discharge initiation.

was computed for conditions typical of electric-discharge-pumped KrF* lasers.[3] The results of this calculation are presented in Fig. 1 as a function of F_2 fractional concentration. For values of X_{F_2} below about 0.002 electron energy loss due to dissociation is found to be relatively unimportant. However, for higher F_2 concentrations the electron energy loss accompanying dissociation can become very significant, exceeding 10% of the total discharge power. For the conditions of Fig. 1 the rate coefficient for direct dissociation has a value of approximately 10^{-9} sec^{-1} cm^3 and exhibits a weak dependence on E/n. Since the production of rare gas metastable states is a strong positive function of E/n, the fractional power transfer associated with the direct dissociation process decreases relative to rare gas metastable production for E/n values higher than 1.0×10^{-16} V cm^2 and increases for lower values.

Although the cross sections for F_2 vibrational excitation are relatively large,[1] Fig. 1 shows that the electron energy loss due to vibrational excitation is not likely to be important since the energy loss per collision is small (~0.1 eV). However, Hall's results[1] indicate that dissociative attachment increases significantly with F_2 vibrational level. In long-pulse[3] KrF* laser discharges the fraction of vibrationally excited F_2 will be substantial (>10%). Thus, the degree of F_2 vibrational excitation may affect the electron loss due to attachment, thereby influencing both the quasisteady and stability characteristics of rare gas—halide discharges.

In order to evaluate the influence of the electron-F_2 collision processes discussed above, electron distribution functions and all related Ar and Kr rate coefficients were computed as a function of F_2 fractional concentration. The effects of electron-electron, electron-ion, and electron-metastable collisions were taken into

account in the calculation. The data so obtained were then used as input information in a time-dependent KrF* kinetics model of an electron-beam-sustained discharge,[3] following procedures generally similar to those described elsewhere.[4,5] Figure 2 shows the computed variation of gain and KrF* production efficiency with F_2 fraction. The results presented refer to conditions 100 nsec after discharge initiation. In the present analysis the KrF* production efficiency is defined by the relation $\eta = (\text{KrF}^* \text{ production})h\nu/([\text{Ar}]S_E u_i + JE)$, where all the processes contributing to the *volumetric* rate of KrF* production are included in the numerator.[6] Also, S_E is the rate of electron-ion pair production by the electron beam, u_i is the energy required to produce an electron-ion pair, JE is the discharge power density, and $h\nu$ is the photon energy of the KrF* laser transition. Thus, on this basis η represents the maximum fraction of the total power potentially recoverable from the reaction, $\text{KrF}^* + h\nu \rightarrow \text{Kr} + \text{F} + 2h\nu$.

Interpretation of the specific nature of changes accompanying variation in F_2 concentration can be very difficult for the circumstances typical of most experiments since the halogen molecules influence numerous plasma processes. Therefore, in order to assist in interpretation, in the present calculation the e-beam ionization rate, S_E, was varied from 50 to 500 sec^{-1} as the F_2 fraction was increased from 0.001 to 0.01. Thus, the electron density remains approximately constant at 10^{11} cm^{-3} for the conditions of Fig. 2. In addition, the *total* power density is sensibly constant, increasing from about 60 kW cm^{-3} to 90 kW cm^{-3} over the X_{F_2} range covered.[7] These conditions are representative of recent experiments[3] with electron-beam-sustained rare gas—halide lasers.

As the F_2 fraction is increased above 0.001, Fig. 2 indicates that both the gain and KrF* production efficiency increase significantly. This reflects the improved efficiency of ArF* formation from the rare gas metastable states as compared to other metastable loss processes. However, as X_{F_2} is increased above about 0.005, electron energy loss due to F_2 dissociation becomes increasingly more significant. The resultant cooling of the electrons leads to a 35% decrease in the Ar and Kr metastable production rates for the conditions of this example as X_{F_2} is increased from 0.001 to 0.01. The combined effect of these related processes is a reduction in the KrF* production efficiency.[8] Additionally, F_2 quenching of KrF* exerts an important deleterious influence on the gain at the higher F_2 levels.[9] Results qualitatively similar to those of Fig. 2 were obtained at lower and higher E/n values, although calculations show that the plasma is unstable for E/n values above about 1.2×10^{-16} V cm^2 when the F_2 fractional concentration is below about 0.002.

Although the dominant collision processes generally become quasisteady in times much less than 100 nsec for conditions typical of those represented by the results of Fig. 2, the temporal changes in plasma processes resulting from F_2 dissociation can become very significant. The consequences of F_2 dissociation become particularly important for long-pulse discharges (~1 μsec) and/or high-power loading (>100 kW cm^{-3}).

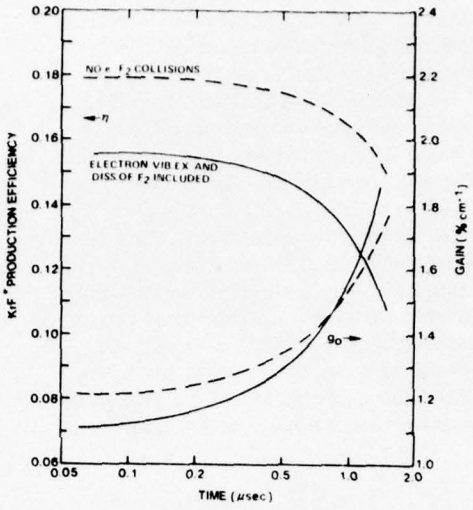

FIG. 3. Temporal variation of KrF* production efficiency and gain for an F_2 fraction of 0.005 and the conditions of Fig. 2. Also shown (dashed curves) are the results of the same calculation neglecting all electron-F_2 collisions except attachment.

Presented in Fig. 3 are the temporal variations of η and g_0 computed for an X_{F_2} value of 0.005, i.e., near-optimum conditions in Fig. 2. For purposes of comparison, also shown are η and g_0 computed neglecting the effects of all electron-F_2 collisions except attachment. Clearly, steady-state conditions are attained in a time less than 100 nsec. However, for times greater than about 0.2 to 0.3 μsec significant changes in both g_0 and η resulting from F_2 dissociation become apparent. The decrease in KrF* production efficiency is a sequence of the increase in electron density accompanying the decrease in F_2 concentration. As the electron density increases, electron excitation of rare gas metastables to higher excited states begins to compete with the desired F_2 reaction leading to the formation of ArF* and KrF*. For this reason the energy utilization efficiency associated with conversion of metastable atoms to rare gas—halide excimers decreases. Note, however, that because of increasing electron excitation, the absolute densities of metastable and rare gas—halide states continue to increase as is reflected by the increasing gain. As the data of Fig. 3 indicate, this sequence of events results in rapidly changing g_0 and η for long discharge duration. At the 1-μsec time the F_2 is 35% dissociated for the conditions of this example.

Comparison of the dashed and solid curves in Fig. 3 shows that direct electron impact dissociation of F_2 may result in significant changes in the magnitude and rate of change of both gain and KrF* production efficiency. However, it is clear that the general trends exhibited by the data in Fig. 3 are not dependent on the inclusion of electron-F_2 collisions. Indeed, at the 1-μsec time only about one-third of the F_2 dissociation results from direct electron impact for the conditions of this example, with ArF* formation, attachment, and F_2 quenching processes accounting for the other two-thirds.

The results and discussion of this paper focus attention on the role of the halogen-bearing molecule as

regards electron and metastable kinetic processes in rare gas–halide lasers. Conditions typical of electron-beam-sustained laser discharges[3] were examined in detail. The influence of F_2 in KrF* lasers was given particular attention because of the availability (albeit limited) of theoretical and experimental data for this molecule. On the basis of this analysis it is reasonable to conclude that electron-halogen processes other than attachment are likely to be important, particularly F_2 electronic excitation leading to dissociation. This finding will most probably have general significance for all rare gas–halide and mercury-halide lasers containing F_2 or other halogenated molecules at fractional concentration levels greater than a few tenths of a percent. Clearly, additional electron scattering data for halogenated molecules would be of considerable value in the modeling and evaluation of rare gas–halide laser properties.

It is a pleasure to acknowledge the helpful comments of R.T. Brown, R.J. Hall, and L.A. Newman.

[1]R.J. Hall, J. Chem. Phys. (to be published).
[2]H.L. Chen, R.E. Center, D.W. Trainor, and W.I. Fyfe, J. Appl. Phys. 48, 2297 (1977).
[3]C.H. Fisher and R.E. Center, Appl. Phys. Lett. 31, 106 (1977).
[4]J.H. Jacob and J.A. Mangano, Appl. Phys. Lett. 28, 724 (1976).
[5]J.A. Mangano, J.H. Jacob, and J.B. Dodge, Appl. Phys. Lett. 29, 426 (1976).
[6]For the conditions of this example the displacement reaction $ArF^* + Kr \rightarrow KrF^* + Ar$ dominates KrF* production (see Ref. 9).
[7]Since the discharge contribution to the total power density was sensibly constant over the entire X_{F_2} range covered in Fig. 2, the discharge enhancement factor, $JE([Ar]u_i S_E)^{-1}$ decreased from about 10 to 1 as X_{F_2} increased from 0.001 to 0.01, reflecting the increase in S_E required to maintain nearly constant electron density. However, the discharge contribution to the total volumetric power density was dominant over most of the range covered in Fig. 2.
[8]Due to the decrease in enhancement factor corresponding to the increase in X_{F_2} for the conditions described here, the discharge is relatively less important at high F_2 fractions; this effect also contributes to the reduction in η.
[9]M. Rokni, J.H. Jacob, and J.A. Mangano, Phys. Rev. (to be published).

Influence of molecular dissociation and degree of ionization on rare gas–halide laser properties[a)]

William L. Nighan

United Technologies Research Center, East Hartford, Connecticut 06108
(Received 29 September 1977; accepted for publication 20 December 1977)

The influence of F_2 dissociation and the accompanying increase in fractional ionization is examined for conditions typical of electron-beam-sustained KrF* lasers. It is found that for electron-density–F_2-density ratios greater than about 10^{-3}, rare-gas metastable loss due to electron excitation of higher levels begins to compete significantly with metastable-F_2 reactions, thereby leading to a substantial reduction in rare gas–halide production efficiency.

PACS numbers: 42.55.Hq, 52.25.–b, 34.80.Dp

Numerous processes contribute to dissociation of the halogen-bearing molecule in rare gas—halide lasers.[1] In long-pulse (~1 μsec) or high-power-density ($\gtrsim$ 100 kW cm^{-3}) lasers the reduction in halogen molecule density can be substantial ($>10\%$). Two of the most significant effects accompanying dissociation are (1) an increase in the rare-gas metastable density due to a decrease in the rate of reactions with the halogen molecule and (2) an increase in the electron density due to the combined effects of reduced attachment loss and increased ionization from rare-gas metastable states. In the present paper the influence of these coupled processes on gain and rare-gas-halide production efficiency is examined for conditions representative of electron-beam-sustained KrF* laser discharges.[2]

In order to evaluate the effect on laser discharge properties of temporal changes in plasma processes, a numerical kinetics model was developed following procedures generally similar to those described elsewhere,[1,3,4] with the following exceptions: (1) In the present analysis the effects of direct electron impact dissociation and vibrational excitation of F_2 were taken into account[1] and (2) the effects of electron-electron[5] and electron-ion collisions were included in the calculation of the electron distribution function and all electron rate coefficients.

For atmospheric-pressure mixtures of Ar, Kr, and F_2 in which the fractional concentration of Ar is approximately 0.95, on the order of 50% of the total electrical power is utilized in the production of argon metastable states.[1,4] The metastable atoms so produced engage in numerous reactions, with the primary reaction sequence leading to KrF* formation,[6] e.g.,

$$Ar^* + F_2 \rightarrow ArF^* + F,$$

$$ArF^* + Kr \rightarrow KrF^* + Ar.$$

For optimum discharge conditions studies show that this energy pathway can be very efficient with as much as 20% of the total power available for conversion to optical energy. However, the present analysis indicates that significant changes in the nature of rare-gas metastable loss accompany the decrease in F_2 concentration due to dissociation. Presented in Fig. 1 are computed time-dependent fractional contributions of various argon metastable loss processes in an atmospheric-pressure electron-beam-sustained KrF* laser discharge. In this example, the electron-ion pair production rate by the electron beam was set so as to produce an initial electron density of approximately 10^{14} cm^{-3}. For these conditions the power input from the e-beam was about one-third of the total power, i.e., the discharge enhancement factor was approximately 3. The results of Fig. 1 show that the two primary loss

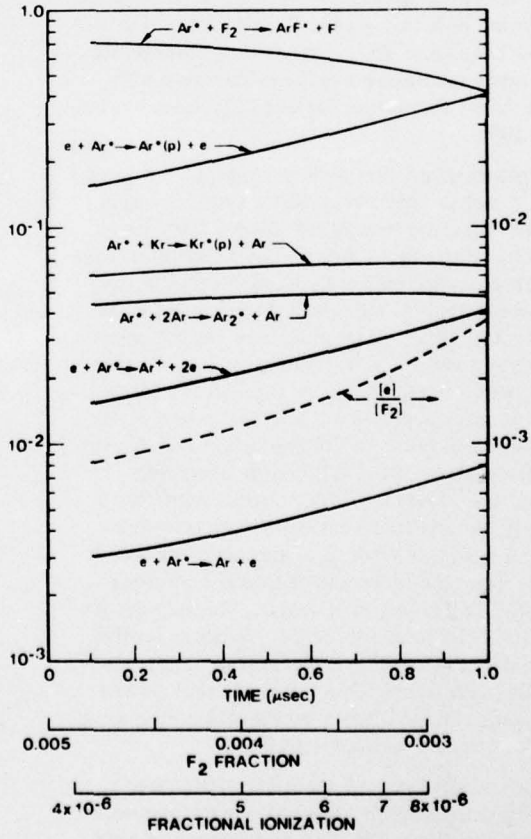

FIG. 1. Fractional contributions to argon metastable atom loss processes in an electron-beam-sustained atmospheric-pressure discharge with an E/n value of 1.2×10^{-16} V cm^2. For these conditions the gas mixture was composed of Ar-Kr-F_2 (0.95-0.05-0.005) and the e-beam electron-ion pair production rate was 250 sec^{-1}.

[a)] Portions of this work were supported by the Office of Naval Research.

 0003-6951/78/3207/0424$00.50

TABLE I. Fractional contributions to F_2 dissociation for the conditions of Fig. 1.

Attachment	$e \rightarrow F_2 \rightarrow F + F^-$	0.14
Direct dissociation	$e + F_2 \rightarrow 2F + e$	0.36
ArF* production	$Ar^* + F_2 \rightarrow ArF^* + F$	0.28
KrF* quenching by F_2	$KrF^* + F_2 \rightarrow$ products	0.12
Other processes		0.10
		1.00

processes controlling the density of argon metastables are the desired F_2 reaction resulting in ArF* formation and electron excitation of the metastables to the rare-gas p states.[7] For times up to about 0.4 μsec Fig. 1 shows that p-state excitation is not particularly significant. However, for longer times electron excitation of metastables to higher states becomes very important. This trend is a direct consequence of the decrease in F_2 concentration due to dissociation which, in turn, results in an increase in electron density. Since the Ar^*-F_2 reaction is a binary process and since the electron-Ar^* p-state excitation rate is very weakly dependent on E/n, the increasing importance of p-state excitation relative to ArF* formation depends almost solely on the relative concentrations of electrons and F_2 molecules. Note that the electron-density–F_2-density ratio, which is also shown in Fig. 1, increases by almost a factor of 5 in 1 μsec. Based on these considerations the results of Fig. 1 show that metastable loss due to p-state excitation begins to compete significantly with ArF* formation for $[e][F_2]^{-1}$ ratios greater than about 10^{-3}.

It is worth pointing out that in this example the initial power density level is only about 70 kW cm^{-3}, a value not much higher than the measured[2] 20-kW cm^{-3} laser threshold levels. Further, Table I shows that there are several processes contributing to F_2 dissociation, any one of which would lead to substantial dissociation on a μsec time scale. Thus, dissociation of the halogen-bearing molecule appears to be of fundamental importance for conditions typical of rare gas–halide lasers. In this regard it is interesting to note that when F_2 is used as the source of fluorine, dissociation results in the gradual elimination of the molecular attaching species. Thus, the resultant effect of dissociation on electron density and electron energy kinetics[1] will be a maximum if a diatomic source of fluorine is used. If a polyatomic fluorine molecule is used, reactions of the type listed in Table I still occur, but they do not appreciably affect the total *molecular* density, so that the kinetic feedback effects of dissociation on the electrons should be much less. This suggests that more-stable longer-pulse discharges may be attainable using polyatomic sources of F rather than F_2.

The potential significance of the effects discussed above is vividly illustrated by the results presented in Fig. 2. This figure shows the E/n dependence of gain and KrF* production efficiency at a time 0.5 μsec after discharge initiation. In this example the production rate of electrons by the electron beam was varied from 125 to 500 sec^{-1} resulting in an increase in the *initial* electron density from approximately 5×10^{13} to 2×10^{14} cm^{-3}; all other parameters including the initial F_2 concentration were held constant. For fixed E/n values below about 1.0×10^{-16} V cm^2, the gain increases and KrF* production efficiency decreases as S_E is increased, reflecting the effect of increased electron density relative to that of the F_2. As the electron density increases, the increased electron pumping rate results in an absolute increase in the densities of both the rare-gas metastables and KrF* as reflected by the higher gain. However, the overall energy utilization efficiency is reduced because electron excitation of rare-gas metastables to higher levels begins to compete with the metastable-F_2 reaction leading to ArF* (Fig. 1). Thus, η decreases as S_E is increased. For a fixed value of the electron-beam ionization rate, increasing E/n initially results in a substantial increase in both gain and KrF* production efficiency due to the strong dependence of rare-gas metastable production on E/n. However, for E/n values greater than about $(1.0-1.2)\times10^{-16}$ V cm^2 the combined influence of increased electron production due to metastable ionization and decreased attachment loss accompanying F_2 dissociation results in an electron density increase. The effect of the resultant increase in the ratio $[e][F_2]^{-1}$ is reflected by a sharp decline in η as rare-gas p-state excitation becomes an important loss of metastables relative to ArF* formation.

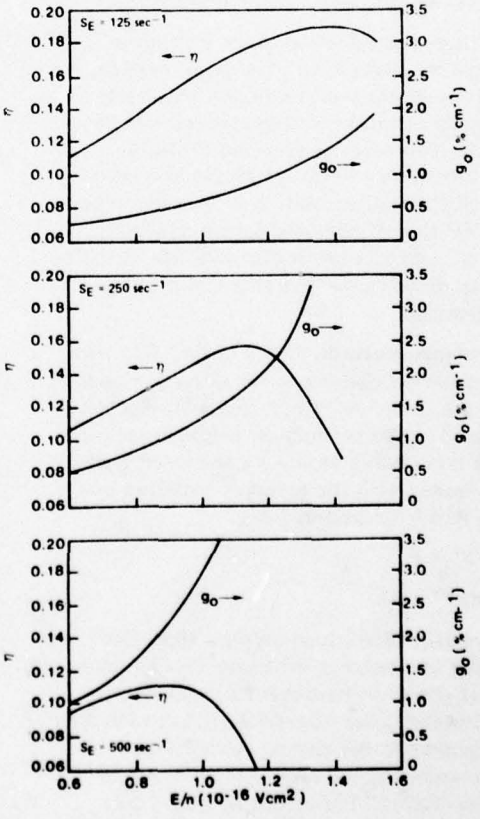

FIG. 2. Computed E/n variation of small-signal gain and KrF* production efficiency for the conditions of Fig. 1 and three values of the e-beam production rate. These results correspond to conditions 0.5 μsec after discharge initiation.

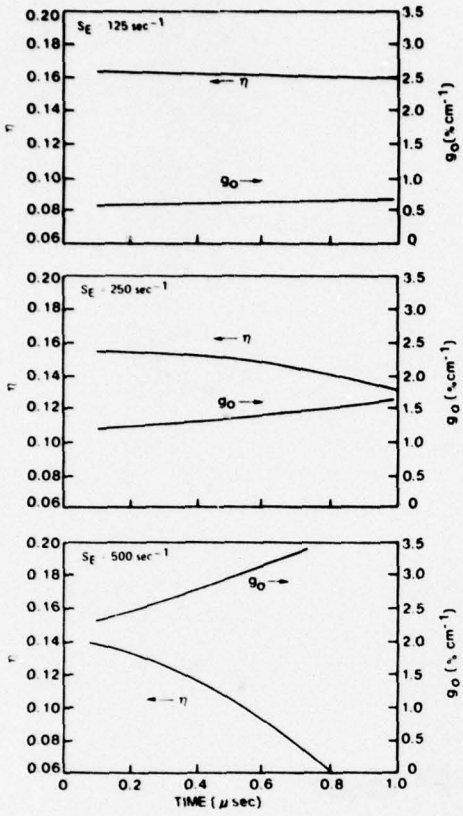

FIG. 3. Temporal variation of small-signal gain and production efficiency corresponding to the conditions of Fig. 2 and an E/n value of 1.0×10^{-16} V cm^2.

For purposes of comparison Fig. 3 shows the temporal variation in η and g_0 at a fixed E/n value of 1.0×10^{-16} V cm^2. For an S_E value of 125 sec^{-1} the total power density is approximately 35 kW cm^{-3} in this example, and both the fractional ionization and F_2 fraction remain sensibly constant at their respective initial values of 2×10^{-6} and 0.005 ($[e][F_2]^{-1} < 10^{-3}$). For this reason both the gain and KrF* production efficiency exhibit little variation on a μsec time scale. This is in sharp contrast to the η and g_0 temporal variation when S_E is increased to 500 sec^{-1}. In this situation the fractional ionization and F_2 fraction change from their initial values of 8×10^{-6} and 0.005 to 1.4×10^{-5} and 0.003 in the first 0.6 μsec. There results an increase in the power density from 155 to 260 kW cm^{-3}, leading ultimately to plasma instability at approximately 0.75 μsec. The corresponding increase in the ratio $[e][F_2]^{-1}$ from 1.6×10^{-3} to 4.7×10^{-3} explains the precipitous temporal decline in KrF* production efficiency.

The previous discussion is based on the assumption that electron excitation of rare gas metastable atoms to the p states results in an unrecoverable loss of energy and of useful excited species, a conservative point of view. However, even if Ar and Kr p states react with F_2 to form ArF* and KrF*, or if electron and heavy particle deexcitation of p-state atoms results in repopulation of metastable states, the 1.5–2.0-eV electron energy loss accompanying p-state excitation from metastable states can be substantial.[1,3] Indeed, for metastable fractional concentrations greater than about 10^{-5} p-state excitation is the dominant electron energy loss process.

The results of this analysis indicate that for F_2 fractions corresponding to a few tenths of a percent, generation of efficient stable long-duration (~1 μsec) rare gas–halide laser discharges requires that the fractional ionization be maintained at a level no higher than approximately 5×10^{-6}. For values of fractional ionization of 10^{-5} and above, the selectivity of energy transfer from the electrons through the rare gas metastable states to the rare gas–halide excimer states is substantially reduced. In addition, for values of fractional ionization above this level electron-electron collisions influence the high-energy region of the electron distribution function,[5] resulting in a very significant increase in the rate of ionization of atoms from their ground state. This effect contributes to the premature occurrence of instability in electron-beam-sustained rare gas–halide laser discharges.

It is a pleasure to acknowledge the helpful comments of R. T. Brown, R. J. Hall, and L. A. Newman.

[1] W. L. Nighan, Appl. Phys. Lett. **32**, 297 (1978).
[2] C. H. Fisher and R. E. Center, Appl. Phys. Lett. **31**, 106 (1977).
[3] J. H. Jacob and J. A. Mangano, Appl. Phys. Lett. **28**, 724 (1976).
[4] J. A. Mangano, J. H. Jacob, and J. B. Dodge, Appl. Phys. Lett. **29**, 426 (1976).
[5] W. H. Long, Appl. Phys. Lett. **31**, 391 (1977).
[6] M. Rokni, J. H. Jacob, and J. A. Mangano, Phys. Rev. (to be published).
[7] In this analysis the rate coefficient for the reaction Ar* + F_2 → ArF* + F was taken as 7.5×10^{-10} sec^{-1} cm^3 [J. E. Velazco, J. H. Kolts and D. W. Setser, J. Chem. Phys. **65**, 3468 (1976)], and the effective rate coefficient representing the net effect of electron excitation and deexcitation of Ar* to and from the p states was taken as 2.0×10^{-7} sec^{-1} cm^3. [See J. L. Delcroix, C. M. Ferreira, and A. Ricard, in *Principles of Laser Plasmas*, edited by G. Bekefi (Wiley, New York, 1976)].

Instability onset in electron-beam-sustained KrF* laser discharges[a)]

Robert T. Brown and William L. Nighan

United Technologies Research Center, East Hartford, Connecticut 06108
(Received 2 February 1978; accepted for publication 21 March 1978)

Measurements of instability onset in a spatially uniform electron-beam-sustained KrF* laser discharge have shown that the time at which instability occurs decreases from about 1 to 0.1 μsec as E/n is increased in the range required for efficient laser operation. This finding is in good agreement with computed ionization instability onset times determined on the basis of a comprehensive model of the discharge.

PACS numbers: 42.55.Hq, 52.35.Py, 52.80.−s

It has been shown[1,2] that the performance of the KrF* laser can be improved by operating with electron-beam-sustained discharge pumping rather than with electron-beam pumping alone. Studies[1-3] have also indicated that the occurrence of discharge instability plays an important role in determining the accessible range of operating parameters for such discharges, thereby exerting a direct influence on the overall performance of a given laser system. In order to obtain a better understanding of the factors leading to discharge instability, we have made detailed measurements of several electron-beam-sustained KrF* discharge properties and have compared the results with predictions of a comprehensive kinetic model. While specifically applicable to externally sustained discharges, the results yield considerable insight and information relevant to the operation of uv-preionized self-sustained discharges as well.

[a)] Portions of the analytical work presented here were supported by the Office of Naval Research.

The experiments were carried out using a 1.5 cm × 2 cm × 50 cm active volume under conditions typical of those corresponding to optimum KrF* laser operation. Discharge pulse length could be varied for times up to 1.0 μsec. Great care was taken in designing the experiment so as to maximize spatial and temporal uniformity of the discharge electric field and of the electron-beam power deposition. The electron beam was produced by a cold-cathode diode operated with a nearly constant 300-kV 1-μsec pulse and a slowly increasing current pulse. The discharge voltage was supplied by a low-inductance capacitor circuit. This circuit was switched on 70 nsec after the start of the electron-beam pulse and produced a temporally uniform 800-nsec voltage pulse, which was terminated 130 nsec prior to the end of the electron-beam pulse. Experimental diagnostics included measurements of the electron-beam voltage and current, discharge voltage and current, discharge fluorescence intensity, and time-integrated photographs of the discharge volume. In

 0003-6951/78/3211-0730$00.50

addition, laser cavity experiments were carried out over a range of parameters.

The discharge cell was constructed using stainless steel, aluminum, and Lucite; Viton O-rings were used throughout. A flat stainless-steel screen was used as the discharge cathode and the anode was a Rogowski-profiled aluminum electrode located 1.5 cm from the cathode. The electron-beam window was an unsupported 1-mil titanium foil 1.5 cm×50 cm in cross section located 0.64 cm behind the discharge cathode screen. Prior to filling with the working gas mixture, the cell was fluorine passivated and was then evacuated to 10^{-5} Torr, using a VacIon pump. The working gas mixture was premixed in a passivated stainless-steel gas-handling system and was replaced after each shot.

Total discharge current was measured by monitoring the voltage drop across a series resistor, and the discharge voltage was measured using a low inductance voltage divider connected directly across the discharge electrodes. The KrF* fluorescence at 248.5 nm was monitored using a fast photodetector (<5 nsec rise time) with a narrow-band (8-nm half-width) filter centered at 248 nm.

Prior to carrying out discharge experiments, a number of tests were performed in order to characterize the electron beam. The diode voltage was monitored using an ammonium chloride voltage divider probe and the total diode current was monitored using a B-dot loop. The electron-beam intensity was measured using both rose cinemoid film and a small scanning Faraday cup and was found to be uniform along the 50-cm dimension to within ±5%. Measurements in air at 1 atm and at a distance 2 cm from the foil window showed that the transverse beam intensity profile was nearly Gaussian, with a half-width of 2.0 cm. In addition, measurements were made in argon at 1 atm with a 1-cm-diam Faraday cup placed 0.7 cm from the discharge cathode screen. These measurements showed that the current density increased linearly by approximately 50% during the 1-μsec pulse and showed small (±15%) fluctuations on a fast time scale (<50 nsec). The measured current density in argon was used to estimate the local electron-beam power deposition by using tabulated stopping powers[4] increased by a factor of 2.5 to account for multiple scattering effects.[5]

In order to identify and understand the primary collisional reactions occurring in the high-pressure (~1 atm) highly ionized ($n_e/n \sim 10^{-6}-10^{-5}$) highly excited ($n^*/n \sim 10^{-5}-10^{-4}$) plasmas of interest, a comprehensive numerical model of the temporal evolution of excited species and discharge properties was utilized.[6] Based on the computed temporal variation of plasma properties, the ionization instability growth (or damping) rate could then be determined for comparison with experiment using procedures generally similar to those described elsewhere.[7]

Typical experimental results, obtained for discharges in a mixture of 94.5% Ar, 5.0% Kr, and 0.5% F_2 at a total pressure of 1 atm, are shown in Fig. 1. For each shot, the electron-beam power deposition (at 0.5 μsec and at the center of the discharge volume) was 20 kW/cm^3, and the electron-beam pulse duration and the discharge voltage pulse duration (i.e., the time between switch-on and switch-off) were held fixed at 1.0 and 0.8 μsec, respectively. The electron-beam voltage and electron-beam current traces indicated a shot-to-shot variation in beam properties of less than ±5%. Examination of the oscilloscope traces presented in Fig. 1 shows that for E/n values below 1.0×10^{-16} V cm^2 in this mixture, the discharge was stable for the full 800 nsec of the applied voltage pulse. However, as the E/n value was incrementally increased in the range 1.0×10^{-16} to 1.8×10^{-16} V cm^2, discharge instability was observed as indicated by the sharp drop in discharge voltage and KrF* fluorescence, and by the sharp rise in discharge current. Figure 1 shows that the instability onset time decreased from approximately 750 to 120 nsec as E/n was increased. Photographs indicated that in each case in which instability occurred during the pulse, one or more large-volume (~1 cm wide) arcs were present and were centered with respect to the transverse (i.e., 2 cm) electron-beam dimension.

Measured and computed values of discharge current density at times prior to the occurrence of instability were found to be in good agreement. In addition, the qualitative trends exhibited by the experimental traces in Fig. 1 were also observed in the calculated current density curves in that for each value of E/n, a time was reached at which current runaway occurred. Over the E/n range from 1.0×10^{-16} to 1.8×10^{-16} V cm^2, for which the average discharge power enhancement relative to that of the electron-beam alone increased from 2 to approximately 6 during the stable portion of the discharge, the KrF* fluorescence enhancement measured relative to that of pure electron-beam pumping was found to vary from 2.1 to 3.5 (Fig. 1), a finding

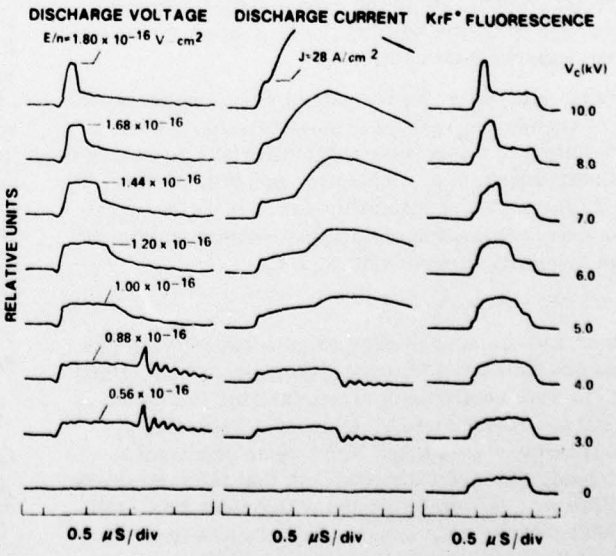

FIG. 1. Discharge voltage, discharge current, and KrF* fluorescence oscillograms for a range of driver charge voltages V_c, and an Ar(0.945)—Kr(0.050)—F_2(0.005) mixture at a pressure of 1 atm.

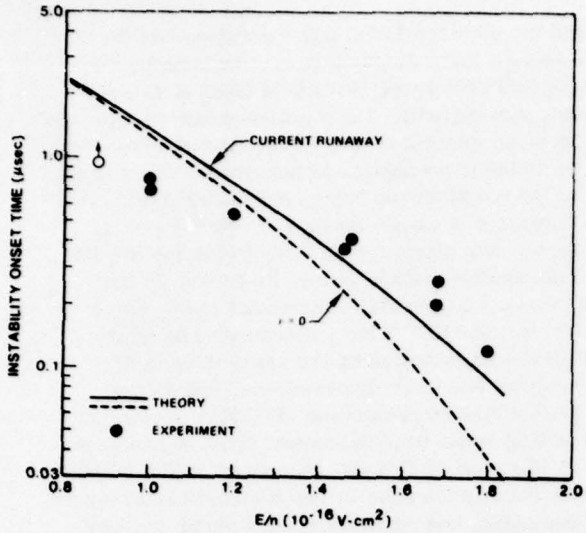

FIG. 2. Instability onset time versus discharge E/n for the conditions of Fig. 1. For $E/n = 0.88 \times 10^{-16}$ V cm^2 the measured onset time exceeded the duration of the applied voltage pulse. The solid curve refers to the time at which runaway of the computed current density occurred, while the dashed curve refers to a self-consistent computation of the ionization instability boundary ($\nu = 0$) as discussed in the text.

which was also in good agreement with predictions of the theoretical model.

Shown in Fig. 2 is the variation of instability onset time with E/n. The experimental points correspond to the time at which the discharge current was first observed to increase sharply as indicated by the oscillograph traces presented in Fig. 1. The solid curve in Fig. 2 corresponds to the instability onset time as evidenced by the occurrence of a sharp rise in the computed discharge current density. Thus, the time of instability onset determined numerically on this basis is directly comparable to the experimental data and, as seen in Fig. 2, the solid curve is in good agreement with the experimental data.

Plasma instability, as indicated by the occurrence of current runaway in rare gas—halide discharges, is a manifestation of temporal amplification of electron density disturbances, i.e., ionization instability. The cause of this mode of instability can be readily appreciated upon examination of an approximate expression[3] for the instability growth rate ν, i.e.,

$$\nu \sim 2n^* k_i^* - n_{F_2} k_a, \tag{1}$$

where n^* and n_{F_2} are the number densities of rare gas metastable atoms and fluorine molecules, while k_i^* and k_a are the rate coefficients for metastable ionization and electron dissociative attachment, respectively. In electron-beam-sustained KrF* laser discharges, initial conditions are established so that the metastable ionization rate is well below the attachment rate, with the result that electron density disturbances are damped ($\nu < 0$). However, there are several processes resulting in F_2 dissociation,[6] including rare gas—halide molecule production. Therefore, as the discharge evolves in time F_2 dissociation proceeds, becoming significant on a time scale less than 1 μsec, with the decreasing F_2 concentration resulting in a reduction in the loss rate of electrons by way of attachment. Consequently, the electron density rises and, additionally, there results an increase in the concentration of rare gas metastables, which are produced by electron impact and lost primarily by reaction with F_2. The combined influence of these processes leads to a strong temporal increase in the metastable ionization rate which rapidly approaches, and then exceeds, the attachment rate, resulting in ionization instability, i.e., $\nu > 0$ [Eq. (1)].

In addition to using the calculated onset of current runaway as a measure of instability, a theoretical criterion for the ionization instability growth (or damping) rate was developed and evaluated as a self-consistent function of plasma properties in the discharge. The effect of ionization of Ar and Kr from their ground states was included in the formulation leading to the expression for the instability growth rate. For the conditions of the present experiment the contribution of ground-state ionization to instability growth was found to be about 10% of that due to metastable ionization. The dashed curve in Fig. 2 represents the E/n variation of the computed ionization instability boundary, defined by the condition $\nu = 0$. Examination of Fig. 2 reveals good agreement between the computed stability criterion (dashed curve) and the numerical indication of current runaway (solid curve). For a relatively long discharge duration (~1 μsec at low E/n), the computed instability onset time and the computed current runaway time are nearly equivalent, reflecting the very short time characteristic of ionization growth (<100 nsec). However, as E/n is increased, the time characteristic of stable discharge duration is reduced to a value comparable to the instability development time ($\sim \nu^{-1}$), and a time delay develops between the onset of instability as defined by the condition $\nu = 0$ and the observation of current density runaway.

Both theory and experiment show that for the conditions compatible with practical electron-beam-sustained KrF* laser devices the occurrence of ionization instability is of a fundamental nature, reflecting the loss of F_2 on a μsec time scale (or less), accompanied by rapid increases in both the metastable and electron densities. Since F atom recombination requires a time much longer than practical KrF* discharge duration times, elimination or circumvention of this problem will probably require means to control the growth of the concentrations of both the metastables and electrons.

It is a pleasure to acknowledge helpful conversations with L. A. Newman, D. C. Smith, and R. H. Bullis.

[1] J. H. Jacob and J. A. Mangano, Appl. Phys. Lett. **28**, 724 (1976).
[2] C. H. Fisher and R. E. Center, Appl. Phys. Lett. **31**, 106 (1977).
[3] J. D. Daugherty, J. A. Mangano, and J. H. Jacob, Appl. Phys. Lett. **28**, 581 (1976).
[4] M. J. Berger and S. M. Seltzer, *Studies in Penetration of Charged Particles in Matter*, Nuclear Science Series Report No. 10, NAS-NRC Publ. 1133 (National Academy of Sciences,

Washington, D.C., 1961).
G.A. Hart and S.K. Searles, J. Appl. Phys. 47, 2033 (1976).
[6]W. L. Nighan, Appl. Phys. Lett. 32, 297 (1978); 32, 414 (1978).
[7]W. L. Nighan, Phys. Rev. A 15, 1701 (1977); 16, 1209 (1977).

Dissociative attachment and vibrational excitation of F_2 by slow electrons[a)]

R. J. Hall

United Techonologies Research Center, East Hartford, Connecticut 06108
(Received 2 September 1977)

Self-consistent dissociative attachment and vibrational excitation cross sections for F_2 have been calculated using Herzenberg's theory of resonant electron scattering. It has been found that the observed electron–F_2 attachment data can be explained by a low energy shape resonance. Potential parameters for the $^2\Sigma_u^+$ negative ion were varied in order to fit predicted attachment cross sections to measured rate constant data. The best fit was obtained for a negative ion curve which crosses the F_2 ground state in the vicinity of the equilibrium internuclear separation, in good agreement with an *ab initio* calculation for this state. The associated total vibrational cross section has a peak of about 2.0×10^{-16} cm^2 at an incident electron energy of 0.45 eV. A strong dependence of attachment rate on F_2 vibrational state is predicted.

I. INTRODUCTION

Molecular fluorine is an important constituent in several electrically-excited gas lasers.[1,2] However, aside from dissociative attachment,[3–6] little is known about low energy electron impact with fluorine. There is reason to expect that the presence of F_2 in a gas mixture will have some effect on electron energy transfer other than dissociative attachment. Inelastic processes such as F_2 vibrational excitation, direct dissociation, or electronic excitation could have important consequences for electrically-excited lasers employing F_2. The vibrational excitation cross section in particular is amenable to analysis, because it and the dissociative attachment cross section can be calculated simultaneously from resonance scattering theory.[7–10] A resonance calculation whose validity has been established by comparison with attachment data will yield additional information about the unknown vibrational excitation cross section.

Ab initio calculations[11] for the $^2\Sigma_u^+F_2^-$ ion indicate that the potential energy curve for this state crosses the ground state near the latter's equilibrium internuclear separation. A shape resonance in low energy electron-F_2 scattering is likely because the lowest vacant antibonding orbital in $F_2(\sigma_u 2p)$ possesses nonzero orbital angular momentum. A spherical harmonic expansion of this orbital has only odd components (p, f, $\cdots$ electrons), and thus a centrifugal barrier, the necessary condition for the existence of a shape resonance, will exist.

In low energy electron-F_2 scattering, the resonance nuclear wavefunction will consist solely of an outgoing wave because there is no turning point at larger internuclear distance to give rise to a reflected wave. Thus, no interference between outgoing and reflected waves can occur, as in the "boomerang" model,[7] and there will consequently be no structure in the F_2 vibrational cross sections as a function of electron energy. This analysis is limited to consideration of a single resonance, $F_2^-(^2\Sigma_u^+)$. At higher electron energies, there is the possibility of contributions from excited states of F_2^-.[12] However, until attachment measurements at higher energy provide evidence that these states are important, it is not advantageous to include them in the calculation.

The details of the resonance scattering theory are presented elsewhere[7,8] with emphasis directed towards N_2 and N_2O. Thus, only the highlights of the model and those aspects relevant to F_2 are discussed here. The fitting of the theory to attachment data is first carried through in a local potential approximation in which the decay of the resonance is assumed to be proportional to the resonance nuclear wavefunction. Because this approximation may be doubtful at thermal energies, the low incident energy regime is re-examined in a nonlocal formulation.

II. RESONANT SCATTERING THEORY

Formally, a nuclear wave equation is solved in terms of a complex potential for the compound state, $F_2^-(^2\Sigma_u^+)$. Because little is known about the real and imaginary parts of the compound state potential, these are treated as adjustable parameters. Adjustments are made to the potential parameters in a trial-and-error fashion until the predicted attachment cross sections reproduce experimental rate constants for this process. This process can be expected to give credible results only if the "best fit" potential parameters are physically realistic.

Calculations for F_2 differ mathematically from those for N_2[7] in several relatively minor respects. Because the assumed F_2 resonance is $p\sigma$, the barrier penetration factor required for the calculation of the resonance width should be the expression appropriate to a p wave, and the vibrational excitation cross section is divided by a factor of 2 because the compound state is nondegenerate [see Eqs. (8) and (12) in Ref. 7]. The boundary condition at infinite internuclear separation is changed from bound state to outgoing wave.

The nuclear wave equation is based upon the adiabatic and local potential approximations. Exchange and spin dependent forces are neglected, leading to

$$\left\{-\frac{\hbar^2}{2M}\frac{\partial^2}{\partial R^2}+W(R)-E\right\}\xi=\zeta'(R)\,\chi_0(R), \tag{1}$$

where $-\hbar^2/2M\times\partial^2/\partial R^2$ is the kinetic energy operator for the nuclei; $W(R)$ is the electronic energy of the com-

[a)]This work was supported by the Office of Naval Research under Contract NO0014-76-C-0847.

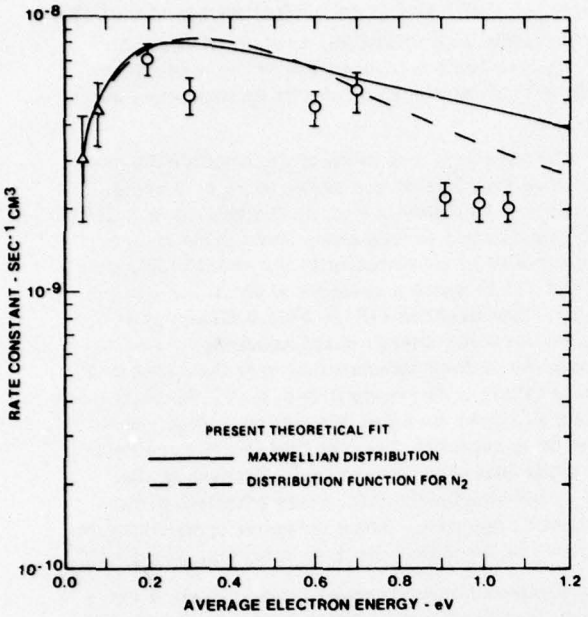

FIG. 1. Fit of resonance scattering theory to experimental attachment data. Solid curve represents rate constant calculated on basis of Maxwellian electron energy distribution. Dashed curve represents use of non-Maxwellian distribution function calculated for N_2-rich mixture. Theoretical attachment cross section from which these rate constants are derived is given in Fig. 2. Experimental data: o—Ref. 3; Δ—Ref. 4.

pound state; E is the total energy (including the zero-point energy); ξ is the wavefunction of the nuclei; $\zeta'(R)$ is an entry amplitude for the incident electron; and $\chi_0(R)$ is the vibrational wavefunction of the target. The compound state energy is represented by

$$W(R) = E^-(R) - \tfrac{1}{2} i\,\Gamma(R), \tag{2}$$

where $\Gamma(R)$ is the autoionization rate multiplied by $\hbar$. Γ is assumed to vary with R in accordance with the penetrability of a p-wave centrifugal barrier[13]

$$\Gamma(R) = \frac{2\gamma(k(R)\rho)^3}{1+(k(R)\rho)^2},$$

where $k(R)$ is the wavenumber of the emitted electron, ρ is the "radius" of the F_2^- ion, and γ is the reduced width. The expression for the entry amplitude ζ' is as given in Ref. 7 [Eq. (14)]

The dissociative attachment cross section is given by the expression,[14]

$$\sigma_{DA} = \frac{V_N}{V_0} g_s \frac{1}{|I_0|^2} \lim_{R\to\infty} |\xi(R, E)|^2, \tag{3}$$

where V_N and V_0 are the nuclear dissociation and incident electron velocities, respectively; g_s is a spin degeneracy factor (unity); and $|I_0|^2$ is the squared amplitude of the incident wave $(8\pi^3)^{-1}$. Cross sections for the vibrational excitation processes,

$$e^- + F_2(v=0) \rightarrow e^- + F_2(v)$$

are calculated from the overlap integral,

$$\sigma_{ov} = \frac{V_v}{V_0} \frac{64\pi^5\mu^2}{\hbar^4} \left| \int dR\, \chi_v^* \zeta \xi \right|^2, \tag{4}$$

where V_v is the velocity of the scattered electron, μ is the electron mass, χ_v is the excited vibrational state wavefunction, and ζ is an exit amplitude for the electron which is set equal to ζ'.[7]

The boundary conditions applied to Eq. (1) are

$$\xi(0, E) = 0$$

$$\lim_{R\to\infty}\left[\frac{d\xi}{dR} - iK\xi\right] = 0 \tag{5}$$

where

$$K^2 = \frac{2M}{\hbar^2} \lim_{R\to\infty} (E - E^-(R)).$$

The two-point boundary value problem (1) and (5) was solved by a conventional centered difference method, with numerical accuracy monitored by evaluating both sides of the equation

$$\frac{\hbar^2 K}{M} \lim_{R\to\infty} |\xi|^2 + \int \Gamma(R) |\xi|^2 dR = -2\,\mathrm{Im} \int \xi^* \zeta' \chi_0 dR \tag{6}$$

which results from multiplying (1) by ξ^*, subtracting the complex conjugate, and integrating.

III. CALCULATED RESULTS

The F_2 ground state potential energy curve was represented by a Morse potential with parameters taken from

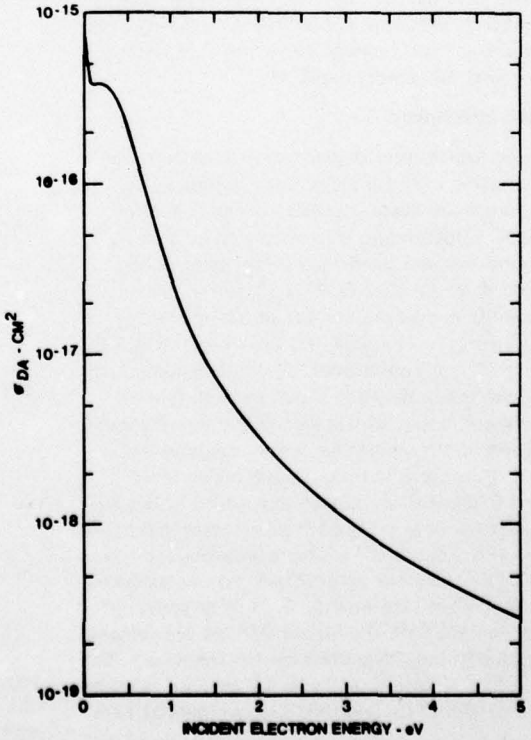

FIG. 2. Best fit attachment cross section as a function of incident electron energy.

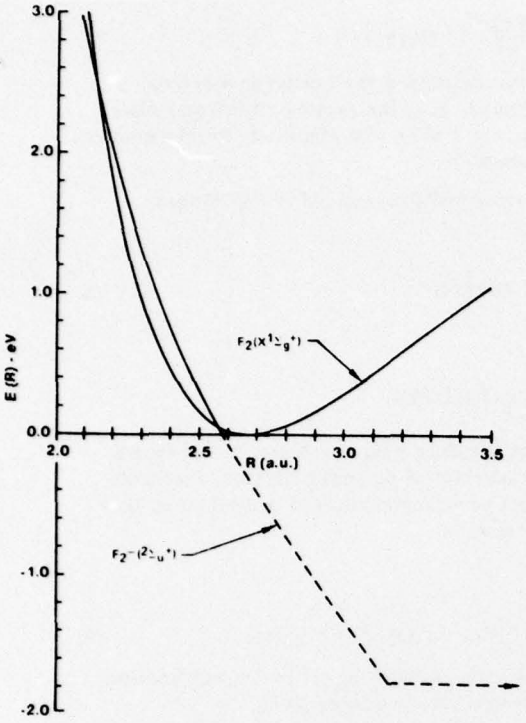

FIG. 3. Real part of best fit compound state potential; ground state represented by Morse potential.

Ref. 15. Morse vibrational wavefunctions were also employed. The real part of the compound state energy was represented by a Taylor series for energies greater than an asymptotic limit deduced from the F_2 electron affinity and ground state well depth.[15]

A. Dissociative attachment

The predicted attachment cross sections were found to be quite sensitive to the internuclear distance, R_s, at which the compound state potential crosses that of the ground state (equilibrium separation R_0). For $R_s \geq R_0$ it was found that the predicted attachment rates, when compared with the data of Refs. 3 and 4, were either too large or had peaks too far displaced from zero electron energy. The best fit, obtained for $R_s < R_0$, is shown in Fig. 1. A non-Maxwellian rate constant calculation has been made because electron distribution function effects are important in one of the experiments. The data of Chen and co-workers[3] were obtained in N_2 buffer gas with F_2 mole fractions on the order of 10^{-3}; departures from Maxwellian due to excitation of the N_2 vibrational mode become important at electron energies around 1 eV. The results of making a non-Maxwellian electron energy distribution attachment rate calculation is shown as the dashed line in Fig. 1.[16] It is apparent that better agreement with the higher energy experimental data is obtained using this distribution function. The fit exhibited in Fig. 1 is judged to be as good as is warranted by the scatter in the available experimental rate data.

The predicted attachment cross section (Fig. 2) has a value of 0.7×10^{-15} cm^2 at an incident energy of 0.01 eV and falls rapidly with increasing energy. A bump at 0.2 eV appears to be a consequence of the approach to zero of the incident electron velocity and the entry amplitude, ζ'.

The real and imaginary parts of the negative ion potential which give this fit are shown in Figs. 3 and 4, respectively. As shown in Fig. 3, the best fit negative ion and ground state curves cross about 0.1 a.u. from R_0. This result is consistent with the *ab initio* calculation of Ref. 11 in which a crossing at about 2.6 a.u. is predicted. The inferred $\Gamma(R)$ in Fig. 4 also is quite reasonable for a low energy shape resonance. Averaging Γ with the nuclear wavefunction over the range $0 < R \leq R_s$ yield values in the range 0.3–0.4 eV. The fact that this width is larger than that for the low energy resonance in O_2 is expected, because this is a p-wave resonance, while that in O_2 is d-wave.[17] Because of the scatter in the attachment data, these potential parameters must be tentative. More extensive measurements, particularly at the higher electron energies, are needed.

If the compound state potential given in Figs. 3 and 4 is correct, the dissociative attachment cross section is likely to have a strong dependence on the vibrational quantum state of the target F_2 molecule. Replacing the $v=0$ wavefunction on the right hand side of Eq. (1) with an excited state target wavefunction and modifying the collision energy make it possible to calculate the v-dependence of the attachment rate. The results of such calculations are presented in Fig. 5, which shows the rates for $v=0$, 1, and 2. The predicted v dependence is very strong, with the peak attachment rate increasing by

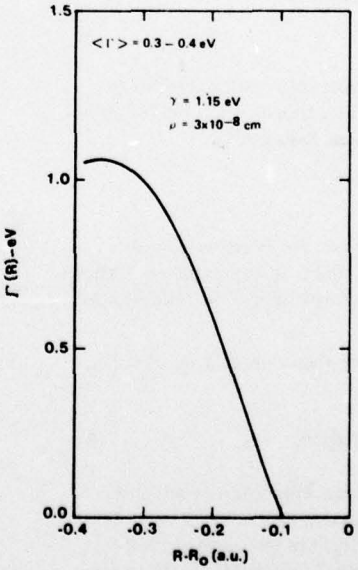

FIG. 4. Imaginary part of best fit compound state potential (the autoionization rate multiplied by $\hbar$). Γ varies with R in accordance with penetrability of p-wave barrier. Averaging Γ over the resonance wavefunction yields values of 0.3–0.4 eV.

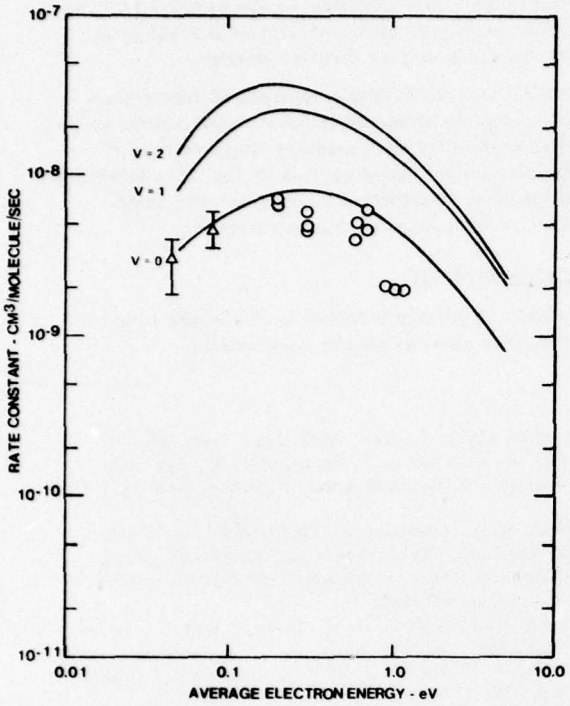

FIG. 5. Predicted dependence of attachment rate on vibrational quantum number of target F_2. Rate constant calculated for Maxwellian electron energy distribution.

about a factor of 5 from $v = 0$ to $v = 2$. This prediction is quite sensitive to the value of R_s; as R_s approaches R_0, the vibrational enhancement is reduced. For $R_s \simeq R_0$, survival factor is a more important consideration than capture, and the predicted rates decrease with increasing v. However, at this point a good fit to the $v = 0$ data could not be obtained.

B. Vibrational excitation

Vibrational excitation cross sections have been evaluated for the best fit attachment case for the process $e^- + F_2(O) \rightarrow e^- + F_2(v)$. Figure 6 shows the calculated cross sections for $v = 1$, 4, 8, and 12, and the sum of the cross sections for excitation up to $v = 15$. The first vibrational state has a peak cross section value of about 10^{-16} cm^2; at $v = 15$ the maximum has fallen to about 0.001 that of $v = 1$. Significant excitation of high lying levels is predicted because this is a "strong coupling" case[14]; the ratio of momentum imparted to the nuclei to the initial r.m.s. momentum, $2a\langle dE^-/dR\rangle/\langle\Gamma\rangle$, is approximately unity. Here a is the vibrational amplitude of the ground state. The lack of structure in these cross sections is due to the absence of reflected components in the nuclear wavefunction.

Because of the scatter in the experimental attachment data, the sensitivity of the vibrational cross sections to reasonable variations in predicted attachment rates has been examined. Repeating the base case calculation with $\gamma = 2.3$ and 0.58 eV ($\langle\Gamma\rangle \simeq 0.7$ and 0.17 eV, respectively) gives rise to a variation in predicted attachment rate that reflects the scatter in the experimental data presented in Fig. 1. The sensitivity of the predicted vibrational excitation cross sections is substantially greater; the cross-section peak at low incident energy is approximately proportional to Γ, with a Γ^2 dependence at high energy. For an attachment cross section as large as that reported in Ref. 5, it is estimated that the predicted peak vibrational cross section would be $O(10^{-14}$ cm^2).

The resonant cross sections shown in Fig. 6 are much larger than those calculated on the basis of direct scattering. Depending on the value assumed for the unknown quadrupole moment derivative, a Born approximation/quadrupole calculation gives a peak cross section of $10^{-20} - 10^{-19}$ cm^2 for the 0–1 transition. Raman scattering data[18] yields a value of 0.21 a.u. for the matrix element of the derived polarizability tensor. Using this value in a polarization potential calculation[19] gives a peak cross section of $10^{-18} - 10^{-17}$ cm^2, depending on the cutoff parameter.

C. Non-local Γ correction

The predictions might be improved at thermal energies by employing a nonlocal Γ formulation.[20] In reality, the term $\Gamma(R)\xi(R)$ in Eq. (1) should be a sum of terms representing negative ion decay to different vibrational states. This effect is accounted for approximately[20,21] by replacing the term $\Gamma(R)\xi(R)$ in (1) by:

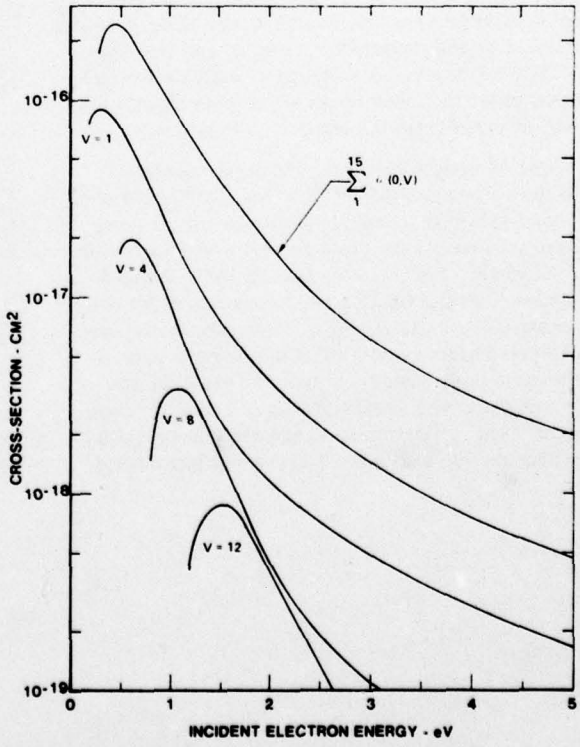

FIG. 6. Predicted vibrational excitation cross sections for target F_2 in $v = 0$ state. Shown are the individual cross sections for excitation of $v = 1$, 4, 8 and 12, and the total vibrational cross section.

$$\sum_v \chi_v(R)\,\Gamma(E-E_v)\int dR'\,\chi_v(R')\,\xi(R',E), \qquad (7)$$

where the v summation extends over open channels and

$$\Gamma(E-E_v)=2\gamma\frac{(k_v\rho)^3}{1+(k_v\rho)^2}$$

$$k_v^2=\frac{2\mu}{\hbar^2}(E-E_v).$$

In the high energy limit the expression (7) returns to $\Gamma(R)\,\xi(R)$. The governing nuclear wave equation (1) thus becomes an integro-differential equation. This equation has been solved iteratively, starting with the ξ wave from the local Γ calculation, for incident energies up to 0.3 eV. The resulting attachment cross section differs little (10%–15%) from that calculated previously. Presumably this is due to the fact that for very low incident energies the decay term is not very important in either case. Thus, the local Γ approximation appears to be adequate for low energy electron-F_2 interactions.

IV. CONCLUSIONS

Resonance scattering theory has been applied to electron-F_2 interactions to calculate self-consistent dissociative attachment and vibrational excitation cross sections. The observed attachment rate data can be explained in terms of a low energy, shape resonance. For a compound state potential that is consistent with *ab initio* calculations, the theory gives a reasonable fit to attachment rate constant data over the range of average electron energies 0.05–1.0 eV. The associated vibrational excitation cross sections for low lying F_2 states have peaks of approximately 10^{-16} cm^2 at electron energies of a few tenths eV. A nonlocal Γ analysis for low incident energies has been found to give results not appreciably different from the local Γ calculation.

The cross section predictions are particularly sensitive to the value selected for R_s. As $R_s \to R_0$, the predicted enhancement of attachment rate by target vibration decreases and changes to a negative dependence at $R_s = R_0$. However, the fit to the data of Refs. 3 and 4 that is obtained by decreasing the resonance width becomes unsatisfactory as $R_s \to R_0$. As negative ion potential parameters are varied over wide ranges, peak attachment rates of slightly less than 10^{-8} cm^3 sec are found to correlate with peak vibrational cross sections of about 10^{-16} cm^2. Variations in the resonance width which reproduce the scatter in the present attachment data suggest that the uncertainty in the predicted vibrational cross section is about a factor of 2 at the peak, and a factor of 4 at higher electron energy.

Note added in proof: Measurements of electron attachment in F_2–He mixtures in the average energy range 3–7 eV have recently been made by Nygaard *et al.*[22] When the attachment cross section of Fig. 2 is integrated over an electron distribution function for He, good agreement is obtained with this new data.[23]

ACKNOWLEDGMENT

The author is greatly indebted to Professor Arvid Herzenberg for several helpful suggestions.

[1] S. K. Searles and G. A. Hart, Appl. Phys. Lett. **27**, 243 (1975); C. A. Brau and J. J. Ewing, *ibid.* **27**, 243 (1975); J. A. Mangano, J. H. Jacob and J. B. Dodge, *ibid.* **29**, 426 (1976).
[2] R. Hofland, M. L. Lindquist, A. Ching, and J. S. Whittier, J. Appl. Phys. **45**, 2207 (1974); R. L. Kerber, A. Ching, M. L. Lindquist, and J. S. Whittier, IEEE J. Quantum Electron., QE-9, 607 (1973).
[3] H. L. Chen, R. E. Center, D. W. Trainor, and W. I. Fyfe, Appl. Phys. Lett. **30**, 99 (1977).
[4] G. D. Sides, T. O. Tiernan, and R. J. Hanrahan, J. Chem. Phys. **65**, 1966 (1976).
[5] P. Mahadevan and R. Hofland, Bull. Am. Phys. Soc. **21**, 575 (1976).
[6] J. J. DeCorpo *et al.*, J. Chem. Phys. **53**, 936 (1970).
[7] D. T. Birtwistle and A. Herzenberg, J. Phys. B **4**, 53 (1971).
[8] L. Dube and A. Herzenberg, Phys. Rev. A **11**, 1314 (1975).
[9] M. Zubek and C. Szmytkowski, J. Phys. B **10**, L27 (1977).
[10] B. I. Schneider, Phys. Rev. A **14**, 1923 (1976).
[11] T. N. Rescigno and C. F. Bender, J. Phys. B **9**, 1329 (1976).
[12] M. V. Kurepa and D. S. Belic, Chem. Phys. Lett. **49**, 608 (1977).
[13] J. M. Blatt and V. F. Weiskopf, *Theoretical Nuclear Physics* (Wiley, New York, 1966), p. 361.
[14] J. N. Bardsley, A. Herzenberg, and F. Mandel, Proc. Phys. Soc. **89**, 321 (1966).
[15] E. A. Colbourn *et al.*, Can. J. Phys. **54**, 1343 (1976).
[16] W. L. Nighan, private communication, June 1977.
[17] D. Spence and G. J. Schulz, Phys. Rev. A **2**, 1802 (1970).
[18] J. M. Hoell *et al.*, J. Chem. Phys. **58**, 2896 (1973).
[19] E. L. Breig and C. C. Lin, J. Chem. Phys. **43**, 3839 (1965).
[20] J. N. Bardsley, J. Phys. B **1**, (1968).
[21] A. Herzenberg, private communication, May 1977.
[22] K. J. Nygaard *et al.*, "Electron Attachment in Fluorine-Rare Gas Mixtures," 30th Gaseous Electronics Conference, Palo Alto, CA, October 19, 1977.
[23] W. L. Nighan, private communication, October 1977.

SEPTEMBER 1976

DISTRIBUTION LIST FOR ONR PHYSICS PROGRAM OFFICE
UNCLASSIFIED CONTRACTS

Director — 3 copies
Defense Advanced Research Projects Agency
Attn: Technical Library
1400 Wilson Blvd.
Arlington, Virginia 22209

Office of Naval Research — 3 copies
Physics Program Office (Code 421)
800 North Quincy Street
Arlington, Virginia 22217

Office of Naval Research — 1 copy
Assistant Chief for Technology (Code 200)
800 North Quincy Street
Arlington, Virginia 22217

Naval Research Laboratory — 3 copies
Department of the Navy
Attn: Technical Library
Washington, D. C. 20375

Office of the Director of Defense — 3 copies
Research and Engineering
Information Office Library Branch
The Pentagon
Washington, D. C. 20301

U. S. Army Research Office — 2 copies
Box CM, Duke Station
Durham, North Carolina 27706

Defense Documentation Center — 12 copies
Cameron Station (TC)
Alexandria, Virginia 22314

Director, National Bureau of Standards — 1 copy
Attn: Technical Library
Washington, D. C. 20234

Commanding Officer — 3 copies
Office of Naval Research Branch Office
536 South Clark Street
Chicago, Illinois 60605

San Francisco Area Office — 3 copies
Office of Naval Research
760 Market Street, Room 447
San Francisco, California 94102

Office of Naval Research — 6 copies
Code 102 1P (ONR/L)
800 North Quincy Street
Arlington, Virginia 22217

Air Force Office of Scientific Research — 1 copy
Department of the Air Force
Washington, D. C. 22209

Commanding Officer — 3 copies
Office of Naval Research Branch Office
1030 East Green Street
Pasadena, California 91101

Commanding Officer — 3 copies
Office of Naval Research Branch Office
495 Summer Street
Boston, Massachusetts 02210

Director — 1 copy
U. S. Army Engineering Research
and Development Laboratories
Attn: Technical Documents Center
Fort Belvoir, Virginia 22060

ODDR&E Advisory Group on Electron Devices — 3 copies
201 Varick Street
New York, New York 10014

New York Area Office — 1 copy
Office of Naval Research
715 Broadway, 5th Floor
New York, New York 10003

Air Force Weapons Laboratory — 1 copy
Technical Library
Kirtland Air Force Base
Albuquerque, New Mexico 87117

Air Force Avionics Laboratory — 1 copy
Air Force Systems Command
Technical Library
Wright-Patterson Air Force Base
Dayton, Ohio 45433

Lawrence Livermore Laboratory — 1 copy
Attn: Dr. W. F. Krupke
University of California
P. O. Box 808
Livermore, California 94550

Harry Diamond Laboratories — 1 copy
Technical Library
Connecticut Ave. at Van Ness, N. W.
Washington, D. C. 20008

Naval Air Development Center — 1 copy
Attn: Technical Library
Johnsville
Warminster, Pennsylvania 18974

Naval Weapons Center — 1 copy
Technical Library (Code 753)
China Lake, California 93555

Naval Training Equipment Center — 1 copy
Technical Library
Orlando, Florida 32813

Naval Underwater Systems Center — 1 copy
Technical Library
New London, Connecticut 06320

Commandant of the Marine Corps — 1 copy
Scientific Advisor (Code RD-1)
Washington, D. C. 20380

Naval Ordnance Station — 1 copy
Technical Library
Indian Head, Maryland 20640

Naval Postgraduate School — 1 copy
Technical Library (Code 0212)
Monterey, California 93940

Naval Missile Center — 1 copy
Technical Library (Code 5632.2)
Point Mugu, California 93010

Naval Ordnance Station — 1 copy
Technical Library
Louisville, Kentucky 40214

Commanding Officer — 1 copy
Ocean Research & Development Activity
National Space Technology Laboratories
Bay St. Louis, Mississippi 39520

Naval Explosive Ordnance Disposal Facility — 1 copy
Technical Library
Indian Head, Maryland 20640

Naval Electronics Laboratory Center — 1 copy
Technical Library
San Diego, California 92152

Naval Undersea Center — 1 copy
Technical Library
San Diego, California 92132

Naval Surface Weapons Center — 1 copy
Technical Library
Dahlgren, Virginia 22448

Naval Ship Research and Development Center — 1 copy
Central Library (Code L42 and L43)
Bethesda, Maryland 20084

Naval Surface Weapons Center — 1 copy
Technical Library
Silver Spring, Maryland 20910

Naval Avionics Facility — 1 copy
Technical Library
Indianapolis, Indiana 46218